Euro. Jnl of Applied Mathematics (2010), *vol.* 21, *pp.* 77–107.
doi:10.1017/S0956792509990155

Particle trapping by an external body force in the limit of large Peclet number: applications to magnetic targeting in the blood flow

G. RICHARDSON[1], K. KAOURI[2] and H. M. BYRNE[2]

[1]*School of Mathematics, University of Southampton, Southampton SO17 1BJ, UK*
e-mail: G.Richardson@soton.ac.uk
[2]*School of Mathematical Sciences, University of Nottingham, Nottingham NG7 2RD, UK*

(*Received 19 February 2009; revised 4 November 2009*)

Motivated by the technology of magnetically targeted drug and gene delivery, in which a magnetic field is used to direct magnetic carrier particles from the circulation to a target site, we develop a continuum model for the motion of particles (magnetic carriers) subject to an external body force (magnetic field) in a flow of a concentrated suspension of a species of neutrally buoyant particles (blood). An advection–diffusion equation describes the evolution of the carrier particles as they advect in the flow under the action of an external body force, and diffuse as a result of random interactions with the suspension of neutrally buoyant particles (shear-induced diffusion). The model is analysed for the case in which there is steady Poiseuille flow in a cylindrical vessel, the diffusive effects are weak and there is weak carrier uptake along the walls of the vessel. The method of matched asymptotic expansions is used to show that carriers are concentrated in a boundary layer along the vessel wall and, further, that there is a carrier flux along this layer which results in a sub-layer, along one side of the vessel, in which carriers are even more highly concentrated. Three distinguished limits are identified: they correspond to cases for which (i) the force is sufficiently weak that most particles move through the vessel without entering the boundary layers along the walls of the vessel and (ii) and (iii) to a force which is sufficiently strong that a significant fraction of the particles enter the boundary layers and, depending upon the carrier absorption from the vessel walls, there is insignificant/significant axial carrier flux in these layers.

1 Introduction

There are many physical processes in which particles suspended in a fluid flow are subject to an external body force leading to their sedimentation; these include magnetic separation (e.g. [9]), magnetically targeted drug and gene delivery (e.g. [2, 3, 6, 12, 18, 19, 20, 21]), as well as separation under gravity (e.g. [5]). In this work we are concerned with the sedimentation of a dilute suspension of particles through a flowing, concentrated suspension of neutrally buoyant particles. This has, in particular, application to the technique of magnetically targeted drug delivery whereby a dilute suspension of magnetic particles are suffused into the blood (a concentrated suspension of neutrally buoyant red blood cells (RBCs)) and then drawn out of suspension, by applying a magnetic field, at a target site within the body. The approach adopted by most authors in treating

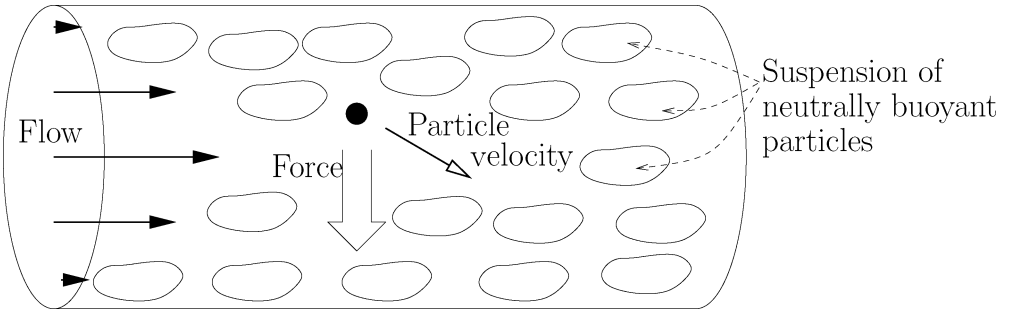

FIGURE 1. A schematic of the set-up under consideration.

problems of this type is to completely neglect the effects of the suspension of neutrally buoyant particles on the sedimenting particles. Since the particle Reynolds numbers we are interested in are small this approximation corresponds to tracking individual particles assuming that the (linear) Stokes drag on each particle balances the applied force responsible for sedimentation (e.g. [8]). However, given that a sedimenting particle will on average have a large number of fluid dynamic interactions with other particles it is sensible to ask what effect this will have on the process. One option would to be simulate the detailed fluid flows around all the particles in the flow and use this to deduce the motion of each individual particle in both suspensions. This is extremely computationally expensive and is unlikely to be justified, in the case of targeted drug and gene delivery, since the information about both the blood vessel geometry and the flow within the vessels lacks detail. The average effect of these interactions can, however, be modelled by a diffusion term proportional to the local shear rate and the resulting effect is commonly termed *shear-induced diffusion* (see e.g. [7, 11, 16, 32]). Thus the motion of sedimenting particles can be described by an advection–diffusion equation. Here the advection term accounts for the particle velocity arising from the drag exerted by the macroscopic flow and the external force applied to the sedimenting particle; the diffusion term describes the effect of the microscopic hydrodynamic interactions of the particle with the concentrated suspension of buoyant particles.

In this work we shall consider an approach based on this advection–diffusion model for the sedimenting particle concentration. In particular we shall be interested in sedimentation (or trapping) onto the absorbing walls of a cylindrical vessel as flow passes through the vessel (see Figure 1) in the limit of large Peclet number (strong sedimentation/weak diffusion). This leads to a regime under which diffusion is negligible in the centre of the vessel while boundary layers form near the vessel wall where there is a balance between diffusion and advection.

There have been a number of works which consider diffusive boundary layers in the large Peclet limit of the advection–diffusion equation. These include: [25] in which internal boundary layers on the separating streamlines between adjacent rolls of a Rayleigh–Bernard convection cell are considered; [1, 15] in which the boundary layer on the edge of a curved two-dimensional obstacle, suspended in an infinite stagnant fluid, is considered and [31] which treats advection–diffusion in a parabolic channel flow. Our analysis bears some similarities to [1, 31]. In particular we find regions of the boundary layer in which

https://doi.org/10.1017/S0956792509990155 Published online by Cambridge University Press

particles tend to become trapped (cf. [1]) and we consider advection of particles in a flow (cf. [31]). There are, however, marked differences in the boundary layer structure we observe from both [1] and [31]. In the former case particles become trapped in re-entrant parts of the boundary that face into the advective velocity where their concentration builds up until the diffusive flux around the boundary layer, out of the re-entrant cup, is sufficient to balance the flux of incoming particles from the bulk of the fluid. In contrast, in our problem, although particles accumulate at the bottom of the cylindrical vessel, these are either advected away by the fluid, along the bottom of the pipe, or absorbed by the walls. In the latter case [31], the boundary is entirely flat and the advective velocity is solely due to the fluid and therefore has no component normal to the boundary.

Before proceeding with the analysis we describe a potentially important application of this analysis, magnetically targeted drug and gene delivery. In conventional systemic drug and gene delivery, the drug (or gene) is administered into the bloodstream and is transported through the circulation around the body and, eventually, to the target site. For relatively small targets (such as a tumour) systemic delivery is extremely inefficient, with a large proportion of the active compound not reaching the target. Various methods have therefore been proposed to enhance uptake at the target site. These include techniques that rely on magnetic targeting using, for example, magnetic microparticles (recently reviewed by Dobson [6] and by Pankhurst *et al.* [21]) and magnetically tagged macrophages (Muthana *et al.* [20]) as the transport vehicle. In the context of the former, and older technology, there have been two Phase I/II clinical trials [18, 28] in addition to numerous *in vivo* studies (e.g. [2, 3, 19]). While the latter, newer technology has only been subject to a single combined *in vitro* and *in vivo* trial [20], it shows great promise. The mathematical modelling of magnetically targeted delivery has been discussed previously by Grief & Richardson [14], by Voltairas *et al.* [27] and Forbes *et al.* [8]. In [8] and [14] magnetic carriers are modelled as a dilute suspension of non-interacting particles while in [27] they are modelled as a ferrofluid (in which magnetic interactions between particles are significant). One reason to suppose that the carrier population is relatively dilute is that, although it may be injected as a concentrated suspension, the effects of Taylor dispersion [24] mean that it disperses widely throughout the cardiovascular system. It thus seems to us that the ferrofluid approach may be overly complicated.

One of our aims is to identify and investigate the dominant mechanisms involved in the targeting process. We remark that the ability of the vessel wall to absorb the targeting particles is key to the success of the process. If, for example, the vessel wall is strongly absorbing then the particles will be trapped in a relatively short distance from their injection site, *even in the absence of a body force*, since shear induced diffusion sets up a flux of particles directed towards the vessel wall. The question that naturally arises is: what advantage does the magnetic force confer? It is clear, for example, that if the vessel wall is strongly absorbing then the body force is largely irrelevant in smaller vessels. However, where the vessel wall absorbs weakly the body force concentrates particles in the vicinity of the wall and thereby significantly aids absorption.

The outline of this work is follows. In Section 2 we formulate a model for the transport of sedimenting particles in a vessel resulting from advection by a body force and shear-induced diffusion. In Sections 3 and 4 we investigate this model using asymptotic methods in the limits of weak diffusion and absorption, finding that the sedimenting particles

concentrate in a boundary layer around the walls of the vessel. In Section 4, in which we consider a scenario in which the flow through the vessel is relatively strong with respect to the trapping force, we find a regular hyperbolic partial differential equation for the particle concentration within this layer, that describes both azimuthal and axial transport of material. In Section 3, where the advective effects from the flow are weaker, there is a singularity in the corresponding transport equation at which charactersitics intersect. Physically this is associated with a sub-layer, which lies to one side of the vessel, into which particles are advected from the adjacent boundary layers. In this layer particle concentration is even higher than in the adjacent boundary layers. Depending upon the level of particle absorption at the vessel walls particles are either absorbed close to where they first enter the boundary layer (high absorption) or they are advected along the vessel for a significant distance (low absorption). In the latter case we derive a simple hyperbolic particle conservation equation for particle concentration in the sub-layer. Finally, in Section 5, we summarise our results and present our conclusions.

2 Problem formulation

We consider a dilute suspension of sedimenting particles, subject to an external body force, and suspended in a flow of a concentrated suspension of a second, neutrally buoyant particulate species. These are subject to an external force which is used to pull them out of circulation at a target site. The sedimenting particles are not only advected in response to the external force and the fluid flow in the pipe but also experience an effective diffusive component to their motion due to their interactions with the suspension of neutrally buoyant particles, that is they undergo shear-induced diffusion [32]. The across-streamline coefficient of diffusion $D(r)$ induced by this effect is well established and takes the form [11, 32]

$$D(r) = K_{sh}(\mathscr{R})^2\dot{\gamma} \quad \text{where} \quad \dot{\gamma} = (2e_{ij}e_{ij})^{1/2}. \tag{2.1}$$

Here r is radial distance measured from the centre of the vessel, $\mathscr{R}$ is the radius of the neutrally buoyant particles, K_{sh} is a dimensionless constant, $\dot{\gamma}$ the shear rate and e_{ij} the rate of strain tensor.

In the absence of diffusion $\boldsymbol{U} = U\boldsymbol{e}_x + V\boldsymbol{e}_y + W\boldsymbol{e}_z$, the velocity of the sedimenting particles, relative to that of the fluid is given by balancing Stokes drag with the external force $\boldsymbol{F}(\boldsymbol{x})$ applied to them, by

$$\boldsymbol{U} = \frac{\boldsymbol{F}(\boldsymbol{x})}{6\pi\mu a},$$

where μ is the effective viscosity of the fluid suspension and a the radius of the particles.

Henceforth we suppose that the trapping occurs in a cylindrical pipe, of circular cross-section, with radius ϱ_v and axis parallel to the z-axis. Furthermore we assume a steady Poiseuille flow in the vessel with velocity $\boldsymbol{v} = \mathscr{U}_0(1 - r^2/\varrho_v{}^2)\boldsymbol{e}_z$. Here $\mathscr{U}_0$ is the maximum velocity of the flow and (r, θ, z) are cylindrical polar coordinates defined in terms of cartesian coordinates, in the usual fashion, by $x = r\cos\theta$, $y = r\sin\theta$ and $z = z$. The assumption of this flow form relies on (I) approximating blood as a Newtonian fluid

https://doi.org/10.1017/S0956792509990155 Published online by Cambridge University Press

(a standard assumption) and (II) neglecting the body force term, in the (fluid) momentum equation, arising from the drag of the sedimenting particles on the fluid – a term retained, for example, in (13) of [9]. For sufficiently dilute suspensions of sedimenting particles the drag force exerted on the fluid is insignificant in comparison to the pressure gradients driving the flow and, in the particular case of magnetically targeted drug delivery, this assumption is appropriate.

In terms of the coordinates defined above and the particle concentration, c, the particle flux, is defined by $\boldsymbol{J} = J_r\boldsymbol{e}_r + J_\theta\boldsymbol{e}_\theta + J_z\boldsymbol{e}_z = -D\nabla c + c(\boldsymbol{U} + \boldsymbol{v})$, where

$$\begin{aligned} J_r &= -D(r)\frac{\partial c}{\partial r} + c(U(\boldsymbol{x})\cos\theta + V(\boldsymbol{x})\sin\theta), \\ J_\theta &= -\frac{D(r)}{r}\frac{\partial c}{\partial \theta} + c(V(\boldsymbol{x})\cos\theta - U(\boldsymbol{x})\sin\theta), \\ J_z &= \frac{c\mathscr{U}_0}{\varrho_v{}^2}(\varrho_v{}^2 - r^2) + cW(\boldsymbol{x}). \end{aligned} \tag{2.2}$$

The corresponding conservation equation for the particle concentration is

$$\frac{\partial c}{\partial t} + \frac{1}{r}\frac{\partial}{\partial r}(rJ_r) + \frac{1}{r}\frac{\partial J_\theta}{\partial \theta} + \frac{\partial J_z}{\partial z} = 0. \tag{2.3}$$

The diffusion coefficient $D(r)$ appearing in (2.2) is derived from (2.1) and for Poiseuille flow we have $D(r) = 2K_{sh}\mathscr{R}^2\mathscr{U}_0 r/\varrho_v{}^2$. On the edge of the vessel we expect particle flux (out through the vessel walls) to be proportional to the particle concentration there; thus

$$J_r|_{r=\varrho_v} = \tilde{\kappa}(z)c|_{r=\varrho_v}, \tag{2.4}$$

where the non-negative function $\tilde{\kappa}(z)$ embodies the permeability of the vessel walls to the sedimenting particles. For generality we allow $\tilde{\kappa}$ to vary with axial distance along the vessel and this might, for example, be used to model the differing permeabilities of a vessel in healthy and diseased (or cancerous) tissue. We also impose the initial and inlet conditions

$$c|_{t=0} = c_0\bar{C}(r,\theta,z), \qquad c|_{z=-Lz_0} = c_0\mathscr{C}(r,\theta,t). \tag{2.5}$$

where c_0 is a typical concentration. Equations (2.2)–(2.5) define a closed system which can be used to determine $c(r,\theta,z,t)$ and, hence, the three components of the flux J_r, J_θ and J_z.

Non-dimensionalisation.
We non-dimensionalise (2.2)–(2.5) as follows:

$$\begin{gathered} \boldsymbol{x} = l\tilde{\boldsymbol{x}}^*, \qquad r = \varrho_v r^*, \qquad z = lz^*, \qquad c = c_0 c^*, \\ t = \frac{l}{\mathscr{U}_0}t^*, \qquad \boldsymbol{U} = \frac{F_0}{6\pi\mu a}\boldsymbol{U}^*, \qquad \boldsymbol{F} = F_0\boldsymbol{F}^*, \\ J_r = \frac{c_0\varrho_v\mathscr{U}_0}{l}J_r^*, \quad J_\theta = \frac{c_0\varrho_v\mathscr{U}_0}{l}J_\theta^*, \quad J_z = c_0\mathscr{U}_0 J_z^*. \end{gathered}$$

https://doi.org/10.1017/S0956792509990155 Published online by Cambridge University Press

Here ϱ_v is the vessel radius, $\mathscr{U}_0$ the maximum flow speed down the vessel, F_0 is a typical value for the force exerted on a particle and l is a typical axial length scale (e.g. the length of the vessel).

We remark that by scaling $\boldsymbol{x}$ with l we are implicitly assuming that variations in the particle body force $\boldsymbol{F}(\boldsymbol{x})$ occur over the typical axial length scale. Later, we shall exploit the disparity in scales between the radius and axial length of the vessel, assuming that $\varrho_v \ll l$ (see Sections 3 and 4). On defining new variables $\Omega(\cdot)$ and $\alpha(\cdot)$ by

$$U^*(\tilde{\boldsymbol{x}}^*) = \Omega(\tilde{\boldsymbol{x}}^*)\sin(\alpha(\tilde{\boldsymbol{x}}^*)), \qquad V^*(\tilde{\boldsymbol{x}}^*) = -\Omega(\tilde{\boldsymbol{x}}^*)\cos(\alpha(\tilde{\boldsymbol{x}}^*)),$$

(so that $\Omega^2 = U^{*2} + V^{*2}$ and $\tan\alpha = U^*/V^*$) and non-dimensionalising we obtain

$$\begin{aligned}
&\frac{\partial c^*}{\partial t^*} + \frac{1}{r^*}\frac{\partial}{\partial r^*}(r^* J_r^*) + \frac{1}{r^*}\frac{\partial J_\theta^*}{\partial \theta} + \frac{\partial J_z^*}{\partial z^*} = 0,\\
&J_z^* = c^*(\delta\lambda W^*(\tilde{\boldsymbol{x}}^*) + (1 - r^{*2})),\\
&J_r^* = -\epsilon\lambda r^*\frac{\partial c^*}{\partial r^*} - \lambda c^*\Omega(\tilde{\boldsymbol{x}}^*)\sin(\theta - \alpha(\tilde{\boldsymbol{x}}^*)),\\
&J_\theta^* = -\epsilon\lambda\frac{\partial c^*}{\partial \theta} - c^*\lambda\Omega(\tilde{\boldsymbol{x}}^*)\cos(\theta - \alpha(\tilde{\boldsymbol{x}}^*)),
\end{aligned} \tag{2.6}$$

subject to

$$J_r^*|_{r=1} = \kappa(z^*)c|_{r=1}, \quad c^*|_{z^*=-z_0} = \mathscr{C}(r^*, \theta, t^*), \quad c^*|_{t^*=0} = \bar{C}(r^*, \theta, z^*), \tag{2.7}$$

where $\boldsymbol{F}^* = \boldsymbol{U}^* = \Omega\sin\alpha\boldsymbol{e}_x - \Omega\cos\alpha\boldsymbol{e}_y + W^*\boldsymbol{e}_z$ and

$$\boldsymbol{x} = z\boldsymbol{e}_z + \delta r(\cos\theta\boldsymbol{e}_x + \sin\theta\boldsymbol{e}_y). \tag{2.8}$$

In (2.6)–(2.8) the dimensionless parameters are defined by

$$\epsilon = \frac{12\pi\mu a K_{sh}\mathscr{R}^2 U_0}{F_0{\varrho_v}^2}, \qquad \delta = \frac{\varrho_v}{l}, \qquad \kappa(z) = \frac{l\tilde{\kappa}(z)}{\varrho_v\mathscr{U}_0}, \qquad \lambda = \frac{l}{L}.$$

Here ϵ is an inverse Peclet number (relating the rates of transverse particle diffusion and advection), δ represents the aspect ratio of the pipe and $\kappa(z)$ the dimensionless vessel permeability. The characteristic length L is the typical axial distance that a particle is advected downstream before the transverse body force pulls it close to the vessel wall and is defined by

$$L = \frac{6\pi\mu a U_0\varrho_v}{F_0}. \tag{2.9}$$

The parameter λ is thus a crude representation of the trapping efficiency of the particle force, with larger λ corresponding to greater efficiency).

https://doi.org/10.1017/S0956792509990155 Published online by Cambridge University Press

We note that ϵ can be more succinctly expressed by using (2.9) to eliminate F_0 in favour of L to give

$$\epsilon = \frac{2K_{sh}\mathscr{R}^2 L}{\varrho_v{}^3}. \tag{2.10}$$

Henceforth we drop the *s.

Parameter estimates pertaining to magnetically targeted drug delivery.
Consider a targeting process in which particles containing magnetite experience a force from a magnetic field. The force $\boldsymbol{F}$ on a magnetic particle in a field of strength $\boldsymbol{B}$ takes the form (see e.g. [14])

$$\boldsymbol{F} = \frac{m_{sat}L(|\boldsymbol{B}|)}{|\boldsymbol{B}|}(\boldsymbol{B}\cdot\nabla)\boldsymbol{B}, \quad \text{where} \quad L(|\boldsymbol{B}|) = \coth\left(\frac{m_{sat}|\boldsymbol{B}|}{kT}\right) - \frac{kT}{m_{sat}|\boldsymbol{B}|},$$

where the function $L(\cdot)$ is a nonlinear saturating function and can thus be approximated in both (i) the limit $m_{sat}|\boldsymbol{B}|/kT \ll 1$ (in which it is linear in $|\boldsymbol{B}|$) and (ii) the limit $m_{sat}|\boldsymbol{B}|/kT \gg 1$ (in which it tends to 1). Here m_{sat} is the saturation magnetisation of the particle, k is Boltzmann's constant and T is absolute temperature. The former limit (i) is termed the superparamagnetic limit and gives rise to an approximate formula for the force of the form

$$\boldsymbol{F} = \frac{m_{sat}^2}{6kT}\nabla|\boldsymbol{B}|^2$$

while the latter limit (ii) is termed the blocked limit and gives rise to a formula for the force of the form

$$\boldsymbol{F} = \left(\frac{m_{sat}\boldsymbol{B}}{|\boldsymbol{B}|}\cdot\nabla\right)\boldsymbol{B}.$$

Since the particle's saturation magnetisation m_{sat} is proportional to its volume, the former formula is appropriate for small particles (and weak magnetic fields) while the latter is appropriate for large particles (and strong fields).

Henceforth we consider only blocked magnetite particles with permanent moment and denote by ρ the density of magnetite, M its magnetisation per unit unit mass, B_G the typical magnetic field gradient and Υ the percentage of the particle composed of magnetite (recall such particles usually have a biocompatible coat) so that $F_0 = (4/3)\pi a^3\rho M\Upsilon B_G$. It follows that L, the typical axial distance that a particle is advected downstream before the transverse body force pulls it onto the vessel walls, and $\epsilon\varrho_v$, the width of the diffusive boundary layer on the vessel wall, are given by

$$L = \frac{9}{2}\frac{\mu U_0\varrho_v}{M\rho B_G\Upsilon a^2} \qquad \epsilon\varrho_v = \left(\frac{9\mu K_{sh}\mathscr{R}^2}{M\rho\Upsilon}\right)\frac{U_0}{B_G a^2\varrho_v}. \tag{2.11}$$

In what follows we will consider a series of cases in which particles of various sizes with a magnetite volume fraction $\Upsilon = 0.1$ are transported in blood of viscosity

https://doi.org/10.1017/S0956792509990155 Published online by Cambridge University Press

Table 1. *Parameter estimates for different sized magnetic particles in various vessels*

Vessel	l (m)	ϱ_v (m)	U_0 (m s^{-1})	a (m)	L (m)	$\epsilon\varrho_v$ (m)
Artery	10^{-1}	1.5×10^{-3}	10^{-1}	5×10^{-6}	0.4	3×10^{-7}
				10^{-6}	10	8×10^{-6}
				10^{-7}	10^3	8×10^{-4}
Arteriole	7×10^{-4}	1.5×10^{-5}	10^{-2}	5×10^{-6}	4×10^{-4}	3×10^{-6}
				10^{-6}	10^{-2}	8×10^{-5}
				10^{-7}	1	8×10^{-3}
Venule	8×10^{-4}	2×10^{-5}	4×10^{-3}	5×10^{-6}	2×10^{-4}	2×10^{-6}
				10^{-6}	5×10^{-3}	4×10^{-5}
				10^{-7}	0.5	4×10^{-3}
Vein	10^{-1}	2.5×10^{-3}	10^{-1}	5×10^{-6}	0.7	2×10^{-7}
				10^{-6}	20	5×10^{-6}
				10^{-7}	2×10^3	5×10^{-4}

$\mu = 4 \times 10^{-4}$ kg m^{-1} s^{-1}, composed of RBCs of radius $\mathscr{R} = 4 \times 10^{-6}$ m and with shear-induced diffusion parameter $K_{sh} = 5 \times 10^{-2}$ [32]. Furthermore we take the magnetisation and density of the magnetite to be $M = 50$ Amp m^2 kg^{-1} and $\rho = 5 \times 10^3$ kg m^{-3}, respectively [6] and assume a magnetic field gradient $B_G = 10$ T m^{-1}. Using these data, taking typical sizes for small arteries, arterioles and small veins, and substituting into (2.11) we obtain the estimates of L and $\epsilon\varrho_v$ presented below in Table 1 wherein l is the typical vessel length.

We remark that l, the typical length of the vessel, is only comparable to L for the largest size of particles ($a = 5 \times 10^{-6}$ m), these being close in size to the upper limit tolerated by the body without causing embolisms [6]. However, even if a significant fraction of carrier particles are not trapped in a single pass through the vessel, this may not significantly undermine the therapy since each vessel is part of a network of vessels of disparate sizes and, furthermore, the carrier particles may recirculate through the targeted region a number of times before being absorbed by the liver. Thus $L \leqslant O(l)$ is not a necessary condition for significant trapping to occur.

We note that the width of the boundary layer around the wall of the vessel (in which diffusive effects balance advective effects) is of size $\epsilon\varrho_v$. Thus the asymptotic analysis may not be valid for sedimenting particle size $a \gg \epsilon\varrho_v$. Nevertheless we expect it to provide results which are at least qualitatively, if not quantitatively, correct when $a = O(\epsilon\varrho_v)$. We remark also that the width of the boundary layer depends inversely on the magnetic field gradient and so increases as the field strength decreases. Thus this analysis maybe more relevant to certain areas of the target site than to others depending on the local strength of the magnetic field gradient.

Expansions of $\Omega(\tilde{\boldsymbol{x}})$, $W(\tilde{\boldsymbol{x}})$ and $\alpha(\tilde{\boldsymbol{x}})$ for $\delta \ll 1$.

In line with the estimates presented in Table 1 we consider the case for which the vessel radius ϱ_v is much smaller than the axial length scale l so that the aspect ratio $\delta \ll 1$. Furthermore we assume that the forces acting on the particles also vary over an $O(l)$ length scale (or bigger) so that they are approximately constant across a pipe cross-section. It

https://doi.org/10.1017/S0956792509990155 Published online by Cambridge University Press

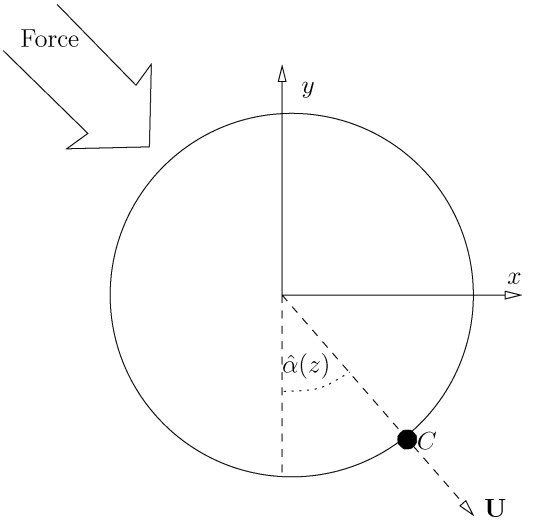

FIGURE 2. The cross-section of the vessel for a particular value of z showing the position of the curve C.

follows that when we expand $\Omega(\tilde{\boldsymbol{x}})$, $W(\tilde{\boldsymbol{x}})$ and $\alpha(\tilde{\boldsymbol{x}})$ as power series in δ the leading-order terms of $\alpha(\boldsymbol{x})$, $W(\boldsymbol{x})$ and $\Omega(\boldsymbol{x})$ (i.e. $\hat{\alpha}$, $\hat{W}$, $\hat{\Omega}$, respectively) are simply functions of z alone. Rather than define $\hat{\alpha}(z)$, $\hat{W}(z)$ and $\hat{\Omega}(z)$ to be the values of α, W and Ω along the centreline of the vessel it proves expedient to define them along the curve C lying on the outer edge of the vessel, to which the force is directed (see Figure 2). In turn this curve is associated with a nested boundary layer (region II) in which particles tend to accumulate. The equation for the curve C is $\boldsymbol{x} = \boldsymbol{q}_c(z) = (\delta \sin\hat{\alpha}(z), -\delta\cos\hat{\alpha}(z), z)$. It follows that $\hat{\alpha}(z)$ and $\hat{\Omega}(z)$ are defined by

$$\hat{\alpha}(z) = \alpha(\boldsymbol{q}_c(z)), \qquad \hat{W}(z) = W(\boldsymbol{q}_c(z)), \qquad \hat{\Omega}(z) = \Omega(\boldsymbol{q}_c(z)). \tag{2.12}$$

Taylor expanding throughout the bulk of the vessel (which has width $O(\delta)$) in powers of δ gives

$$\alpha(\boldsymbol{x}) = \hat{\alpha}(z) + O(\delta), \qquad W(\boldsymbol{x}) = \hat{W}(z) + O(\delta), \qquad \Omega(\boldsymbol{x}) = \hat{\Omega}(z) + O(\delta), \tag{2.13}$$

whilst in the nested boundary layer (region II), which has width $O(\delta\epsilon^{1/2})$,

$$\begin{gathered}\alpha(\boldsymbol{x}) = \hat{\alpha}(z) + \delta\epsilon^{1/2}a_1(z)\eta + O(\delta\epsilon), \qquad W(\boldsymbol{x}) = \hat{W}(z) + O(\delta\epsilon^{1/2}),\\ \Omega(\boldsymbol{x}) = \hat{\Omega}(z) + O(\delta\epsilon^{1/2}).\end{gathered} \tag{2.14}$$

where $a_1(z) = \nabla\alpha\cdot(\boldsymbol{e}_x\cos\hat{\alpha} + \boldsymbol{e}_y\sin\hat{\alpha})$ and $\epsilon^{1/2}\eta = \theta + \pi/2 - \hat{\alpha}(z)$.

3 Matched asymptotic solution in the case of small inverse Peclet number ($\epsilon \ll 1$) and significant trapping efficiency ($\lambda = O(1)$)

Below we consider two distinguished limits of the $\epsilon \ll 1$, $\lambda = O(1)$ regime corresponding to different vessel permeabilities (we consider the case for which λ is small in Section 4).

https://doi.org/10.1017/S0956792509990155 Published online by Cambridge University Press

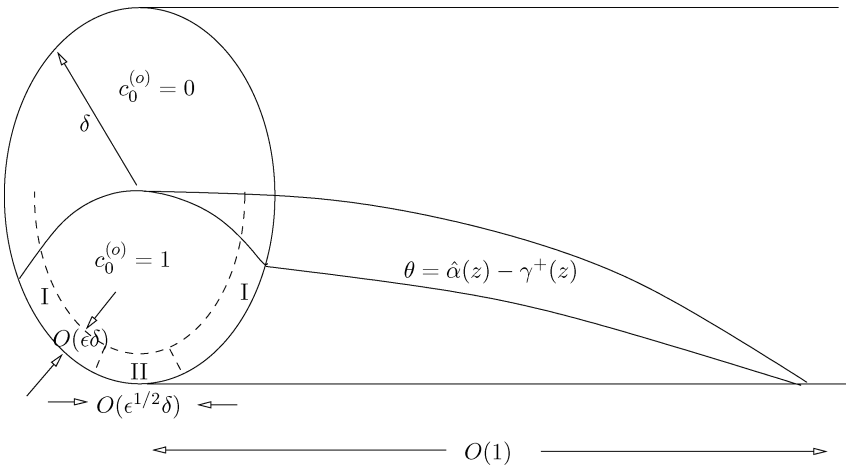

FIGURE 3. A schematic illustrating the asymptotic regions associated with the problem. Dimensions are measured in terms of the typical axial distance down the vessel.

For the two distinguished limits of interest we show that the transport of material in the central section of the pipe (sufficiently far from the walls) is identical to leading order, being dominated by advection (the diffusive terms being negligible). Additionally, in each limit, a diffusive boundary layer develops in a region an $O(\epsilon)$ distance from those parts of the vessel wall to which the advective velocity transports material (region I in Figure 3). In this boundary layer the radial advective flux balances the radial component of the diffusive flux. There is however significant transport of material in the azimuthal (θ) direction towards a point on the boundary corresponding to the curve C in Figure 2. In a neighbourhood of this curve there is a further boundary layer in which there is a balance between diffusive and advective fluxes in the θ direction (region II in Figure 3).

The main difference between the two limits that we consider is that in the first (Section 3.2, $\kappa = O(\epsilon)$) material passes through the walls so quickly that no significant flux develops along the pipe (in the z direction). By contrast the axial flux that develops in the second limit (Section 3.3, $\kappa = O(\epsilon^2)$) transports significant amounts of material away in a thin 'rivulet' running along the curve C. The analysis performed in Section 3.3 leads to a partial differential equation (PDE) describing the evolution of the concentration of material in this rivulet. This enables us to determine material deposition as a function of distance along the vessel.

From a mathematical point of view it is convenient to assume $\delta = O(\epsilon)$ as this is the limit in which the axial particle velocity (in the rivulet) arising from advection by the fluid is of the same order of magnitude as that arising from the particle body force. The choice $\kappa = O(\epsilon^2)$ corresponds to a limit for which particle deposition onto the walls of the vessel depletes particle concentration over an $O(1)$ (dimensionless) length scale, i.e. the same length scale over which significant numbers of particles are removed from the main flow and into the boundary layers on the edge of the vessel. Needless to say, this distinguished limit ($\delta = O(\epsilon)$, $\kappa = O(\epsilon^2)$) has a considerably wider range of applicability

https://doi.org/10.1017/S0956792509990155 Published online by Cambridge University Press

than its strict mathematical definition suggests and we will discuss its domain of validity in the conclusions (Section 5). We remark further that in the first distinguished limit $\kappa = O(\epsilon)$ we also choose $\delta = O(\epsilon)$ in order to be consistent with the second distinguished limit (its choice is largely irrelevant, provided it is small).

We begin our analysis in Section 3.1 by considering the outer region (away from the vessel walls) which is identical, at leading order, for all values of the vessel permittivity κ. We then analyse the distinguished limits $\delta = O(\epsilon)$, $\kappa = O(\epsilon)$ in §3.2 and $\delta = O(\epsilon)$, $\kappa = O(\epsilon^2)$ in Section 3.3.

3.1 Solution structure in the outer region

In this region it is not necessary to rescale variables. We simply consider an asymptotic expansion for $c = c^{(o)}$ of the form

$$c^{(o)} = c_0^{(o)} + \epsilon c_1^{(o)} + \cdots. \tag{3.1}$$

Substituting from (3.1) into (2.6) and transforming to cartesian coordinates ($x = r\cos\theta$, $y = r\sin\theta$) gives the following problem for $c_0^{(o)}$, at leading order,

$$\frac{\partial c_0^{(o)}}{\partial t} + \lambda\hat{U}(z)\frac{\partial c_0^{(o)}}{\partial x} + \lambda\hat{V}(z)\frac{\partial c_0^{(o)}}{\partial y} + (1 - x^2 - y^2)\frac{\partial c_0^{(o)}}{\partial z} = 0,$$

where $\hat{U}(z) = \hat{\Omega}(z)\sin\hat{\alpha}(z)$ and $\hat{V}(z) = \hat{\Omega}(z)\cos\hat{\alpha}(z)$. This first-order linear PDE can be solved by using the method of characteristics in conjunction with the following boundary and initial conditions

$$c_0^{(o)}|_{t=0} = \bar{C}(r,\theta,z), \quad c_0^{(o)}|_{z=-z_0} = \mathscr{C}(r,\theta,t), \quad c_0^{(o)}|_{r=1} = 0 \quad \text{where} \quad (\hat{U}\boldsymbol{e}_x + \hat{V}\boldsymbol{e}_y)\cdot\boldsymbol{e}_r < 0,$$

which are derived from (2.7a)–(2.7c). Henceforth, for simplicity, we fix $\mathscr{C} = 1$ and $\bar{C} = 0$. In this case the domain of solution divides into a region in which $c_0^{(o)} = 1$ and another where $c_0^{(o)} = 0$ and, for sufficiently long times, the solution is time independent. The steady solution to this problem, for a uniform (gravitational) force ($\hat{U} = 0$, $\hat{V} = -g$) was derived by Pich [22]. Since this problem is first order in the spatial derivatives, in contrast to the original problem which was second order, we expect to introduce boundary layers, in which effects from the higher order diffusive terms are significant, in order to satisfy the boundary data on the edge of the vessel.

The eventual position of particles deposited onto the vessel wall is crucially dependent on the parameter κ in (2.7a), larger values being associated with rapid deposition. The solution in the outer region is consistent with particles being withdrawn from the suspension into the vicinity of the vessel wall. For relatively small values of κ (small wall permeability) a high concentration of particles may be established in the immediate vicinity of the wall, in a narrow boundary layer region wherein the advective flux (onto the wall) balances the diffusive flux (away from it).

https://doi.org/10.1017/S0956792509990155 Published online by Cambridge University Press

3.2 The distinguished limit $\delta = O(\epsilon)$, $\kappa = O(\epsilon)$ and $\lambda = O(1)$

3.2.1 *Region I: the diffusive boundary layer on the outflow boundary ($-\pi + \hat{\alpha} < \theta < \hat{\alpha}$)*

In order to balance the advective flux onto the wall with the diffusive flux away from the wall we introduce the scaled radial coordinate R defined by

$$r = 1 - \epsilon R \tag{3.2}$$

and rescale κ and δ by introducing the $O(1)$ parameters κ_1 and Δ

$$\kappa = \epsilon\kappa_1, \qquad \delta = \Delta\epsilon.$$

In terms of the above, rescaling (2.6)–(2.7) can be written as

$$(1-\epsilon R)\frac{\partial c^{(I)}}{\partial t} - \frac{1}{\epsilon}\frac{\partial}{\partial R}\left((1-\epsilon R)J_r^{(I)}\right) + \frac{\partial J_\theta^{(I)}}{\partial \theta} + (1-\epsilon R)\frac{\partial J_z^{(I)}}{\partial z} = 0, \tag{3.3}$$

where

$$J_r^{(I)} = \lambda\frac{\partial c^{(I)}}{\partial R} + \lambda\hat{\Omega}(z)\sin(\hat{\alpha}(z)-\theta)c^{(I)} + O(\epsilon c^{(I)}), \tag{3.4}$$

$$J_\theta^{(I)} = -\lambda\hat{\Omega}(z)\cos(\hat{\alpha}(z)-\theta)c^{(I)} + O(\epsilon c^{(I)}), \tag{3.5}$$

$$J_z^{(I)} = \epsilon c^{(I)}\left(\lambda\Delta\hat{W}(z) + 2R\right) + O(\epsilon c^{(I)}), \tag{3.6}$$

subject to

$$J_r^{(I)}|_{R=0} = \kappa_1\epsilon c^{(I)}, \tag{3.7}$$

and

$$c^{(I)} \to c_0^{(o)}(1,\theta,z,t) \quad \text{as} \quad R \to +\infty, \tag{3.8}$$

where we denote variables in this region by the superscript (I). Condition (3.8) is obtained by matching to the leading-order outer solution and using the expansions of $\alpha(\boldsymbol{x})$, $W(\boldsymbol{x})$ and $\Omega(\boldsymbol{x})$ provided in (2.13). In (3.3) we retain $J_r^{(I)}$, $J_\theta^{(I)}$ and $J_z^{(I)}$, despite being able to express these quantities in terms of $c^{(I)}$; we do this in order to simplify the analysis and to highlight the physical nature of the problem.

Motivated by the fact that the flux of material entering from the outer region is of $O(1)$ and the thickness of region I is of $O(\epsilon)$ we look for an asymptotic solution in which $c^{(I)} = O(1/\epsilon)$ by expanding inner variables as follows:

$$c^{(I)} = \frac{c_0^{(I)}}{\epsilon} + c_1^{(I)} + \cdots,\ J_r^{(I)} = \frac{J_{r,0}^{(I)}}{\epsilon} + J_{r,1}^{(I)} + \cdots,\ J_\theta^{(I)} = \frac{J_{\theta,0}^{(I)}}{\epsilon} + \cdots,\ J_z^{(I)} = J_{z,0}^{(I)} + \cdots. \tag{3.9}$$

Substituting from (3.9) into (3.3) and (3.7) gives, to leading order,

$$\frac{\partial J_{r,0}^{(I)}}{\partial R} = 0, \quad J_{r,0}^{(I)}|_{R=0} = 0 \Longrightarrow J_{r,0}^{(I)} = 0.$$

This result, together with the leading-order expansion of (3.4), implies a balance between diffusive and advective fluxes in the radial direction (at leading order)

$$\frac{\partial c_0^{(I)}}{\partial R} + \hat{\Omega}(z)\sin(\hat{\alpha}(z)-\theta)c_0^{(I)} = 0$$

https://doi.org/10.1017/S0956792509990155 Published online by Cambridge University Press

so that $c_0^{(I)}$ takes the form

$$c_0^{(I)} = A(\theta, z, t) \exp(-\hat{\Omega}(z) \sin(\hat{\alpha}(z) - \theta)R), \tag{3.10}$$

where the amplitude A remains to be determined. We remark that if $-\pi + \hat{\alpha} < \theta < \hat{\alpha}$ (the range of interest) then $\sin(\hat{\alpha}(z) - \theta) > 0$ so that $c_0^{(I)}$ decays exponentially as $R \to +\infty$.

We seek to determine the amplitude A by continuing to $O(\epsilon)$ in (3.3)–(3.4) and (3.7)–(3.8) where we obtain the following system for $J_{r,1}^{(I)}$:

$$\begin{aligned} \frac{\partial J_{r,1}^{(I)}}{\partial R} &= \frac{\partial c_0^{(I)}}{\partial t} + \frac{\partial J_{\theta,0}^{(I)}}{\partial \theta}, \\ J_{r,1}^{(I)}|_{R=0} &= \kappa_1 c_0^{(I)}|_{R=0}, \qquad J_{r,1}^{(I)} \to \lambda \hat{\Omega}(z) \sin(\hat{\alpha}(z) - \theta) c_0^{(o)}(1, \theta, z, t) \quad \text{as} \quad R \to +\infty. \end{aligned} \tag{3.11}$$

An expression for $J_{\theta,0}^{(I)}$, in terms of A, can be found by substituting (3.10) into the leading term of (3.5)

$$J_{\theta,0}^{(I)} = -\lambda \hat{\Omega}(z) A(\theta, z, t) \cos(\hat{\alpha}(z) - \theta) \exp(-\hat{\Omega}(z) \sin(\hat{\alpha}(z) - \theta)R). \tag{3.12}$$

Integrating (3.11a) between $R = 0$ and $R = \infty$ and applying boundary conditions (3.11b) and (3.11c) yields a solvability condition which takes the form of a hyperbolic PDE for the amplitude A and in which z appears solely as a parameter:

$$\begin{aligned} &\frac{\partial A}{\partial t} - \lambda \hat{\Omega}(z) \sin(\hat{\alpha}(z) - \theta) \frac{\partial}{\partial \theta} \left(\frac{A \cos(\hat{\alpha}(z) - \theta)}{\sin(\hat{\alpha}(z) - \theta)} \right) \\ &\quad = -\kappa_1 A \hat{\Omega}(z) \sin(\hat{\alpha}(z) - \theta) + \lambda \hat{\Omega}^2(z) \sin^2(\hat{\alpha}(z) - \theta) c_0^{(o)}(1, \theta, z, t). \end{aligned} \tag{3.13}$$

The characteristics of this PDE are of the form $t = t_0 - \log(|\sec(\theta - \hat{\alpha}(z)) + \tan(\theta - \hat{\alpha}(z))|)/(\lambda \hat{\Omega}(z))$ where t_0 is a constant selecting a particular characteristic. Information is thus propagated in the positive θ direction for $-\pi + \hat{\alpha}(z) < \theta < -\pi/2 + \hat{\alpha}(z)$ and in the negative θ direction for $-\pi/2 + \hat{\alpha}(z) < \theta < \hat{\alpha}(z)$. There is consequently a singularity on $\theta = -\pi/2 + \hat{\alpha}(z)$ where the characteristics converge.

In what follows it will be informative to rewrite (3.13) in terms of the integrated flux within the boundary layer:

$$\frac{\partial}{\partial t} \left(\int_0^\infty c_0^{(I)} \mathrm{d}R \right) + \frac{\partial}{\partial \theta} \left(\int_0^\infty J_{\theta,0}^{(I)} \mathrm{d}R \right) = -\kappa_1 c_0^{(I)}|_{R=0} + \lambda \hat{\Omega}(z) \sin(\hat{\alpha}(z) - \theta) c_0^{(o)}. \tag{3.14}$$

The steady solution to the amplitude equation (3.13).

We now construct a steady solution to (3.13) for the situation outlined above in which, depending upon position within the pipe, $c_0^{(o)}(r, \theta, z, t)$ takes either the value 0 or 1, with a sharp interface (i.e. a free boundary) separating the regions in which the solution takes these two values (this scenario is illustrated in Figure 3). We suppose that the intersection of this free boundary with the wall of the vessel occurs along the curves $\theta = \hat{\alpha}(z) - \gamma^+(z)$

https://doi.org/10.1017/S0956792509990155 Published online by Cambridge University Press

and $\theta = -\pi + \hat{\alpha}(z) + \gamma^-(z)$ so that

$$c_0^{(o)}|_{r=1} = \begin{cases} 0 & \text{for} \quad \theta > \hat{\alpha}(z) - \gamma^+(z), \\ 1 & \text{for} \quad -\pi + \hat{\alpha}(z) + \gamma^-(z) < \theta < \hat{\alpha}(z) - \gamma^+(z), \\ 0 & \text{for} \quad \theta < -\pi + \hat{\alpha}(z) + \gamma^-(z). \end{cases} \tag{3.15}$$

By writing $\psi = \theta - \hat{\alpha}(z)$ and $A = A(\psi, z)$ it is possible to show that the steady solution to (3.13) is, in this case,

$$A(\psi,z) = \begin{cases} 0 & \text{for} \quad 0 > \psi > -\gamma^+, \\ \dfrac{\hat{\Omega}(z)\sin(-\psi)}{1-\kappa_1/\lambda}\left(\left(\dfrac{\cos\gamma^+(z)}{\cos(-\psi)}\right)^{1-\kappa_1/\lambda} - 1\right) & \text{for} \quad -\dfrac{\pi}{2} < \psi < -\gamma^+, \\ \dfrac{\hat{\Omega}(z)\sin(-\psi)}{1-\kappa_1/\lambda}\left(\left(\dfrac{\cos\gamma^-(z)}{-\cos(-\psi)}\right)^{1-\kappa_1/\lambda} - 1\right) & \text{for} \quad -\dfrac{\pi}{2} > \psi > -\pi + \gamma^-, \\ 0 & \text{for} \quad -\pi < \psi < -\pi + \gamma^-. \end{cases} \tag{3.16}$$

Here we apply the boundary conditions $A|_{\theta=\hat{\alpha}(z)} = 0$ and $A|_{\theta=-\pi+\hat{\alpha}(z)} = 0$ to guarantee zero particle flux at $\theta = -\pi + \hat{\alpha}(z)$ and $\theta = \hat{\alpha}(z)$. We remark that it is consistent to apply these *two* conditions to the steady version of (3.13) (a first-order DE) since its characteristics are directed into the domain of solution from the points $\theta = -\pi + \hat{\alpha}(z)$ and $\theta = \hat{\alpha}(z)$. However this leads to a singularity in the solution on $\theta = \hat{\alpha}(z) - \pi/2$ (i.e. on the curve C) where the two sets of characteristics intersect and at which (3.13) has a singularity. In addition the integrated flux $\int_0^\infty c_0^{(I)} \mathrm{d}R$ changes sign here. In order to regularise the singularity in the amplitude in a neighbourhood of $\theta = -\pi/2 + \hat{\alpha}(z)$ we must introduce a further boundary layer about this point. However since the amplitude is finite at $\theta = -\pi/2 + \hat{\alpha}(z)$ for $\kappa_1/\lambda > 1$ we do not investigate this case further here, concentrating instead on the case $\kappa_1/\lambda < 1$ for which A becomes infinite. Examples of the solution (3.16) are plotted in Figure 4. Finally, we write down the corresponding behaviour for $c^{(I)}$, that is

$$c^{(I)} \sim \begin{cases} 0 & 0 > \psi > -\gamma^+, \\ \dfrac{\hat{\Omega}(z)\sin(-\psi)}{\epsilon(1-\kappa_1/\lambda)}\left(\left(\dfrac{\cos\gamma^+(z)}{\cos(-\psi)}\right)^{1-\kappa_1/\lambda} - 1\right)\exp(-\hat{\Omega}(z)\sin(-\psi)R) & -\dfrac{\pi}{2} < \psi < -\gamma^+, \\ \dfrac{\hat{\Omega}(z)\sin(-\psi)}{\epsilon(1-\kappa_1/\lambda)}\left(\left(\dfrac{\cos\gamma^-(z)}{-\cos(-\psi)}\right)^{1-\kappa_1/\lambda} - 1\right)\exp(-\hat{\Omega}(z)\sin(-\psi)R) & -\dfrac{\pi}{2} > \psi > -\pi + \gamma^-, \\ 0 & -\pi < \psi < -\pi + \gamma^-, \end{cases} \tag{3.17}$$

where $\psi = \theta - \hat{\alpha}(z)$.

Limits and validity of (3.16).

The analysis presented above is asymptotically valid for $\delta = o(1)$, $\kappa/\lambda = o(1)$ and $\lambda \geqslant O(1)$. In particular if $\kappa = o(\epsilon)$ and $\lambda = O(1)$ then (3.16) gives the correct amplitude for the leading-order concentration $c_0^{(I)}$ when κ_1 is set to zero. Furthermore where $\lambda = O(1)$ and

https://doi.org/10.1017/S0956792509990155 Published online by Cambridge University Press

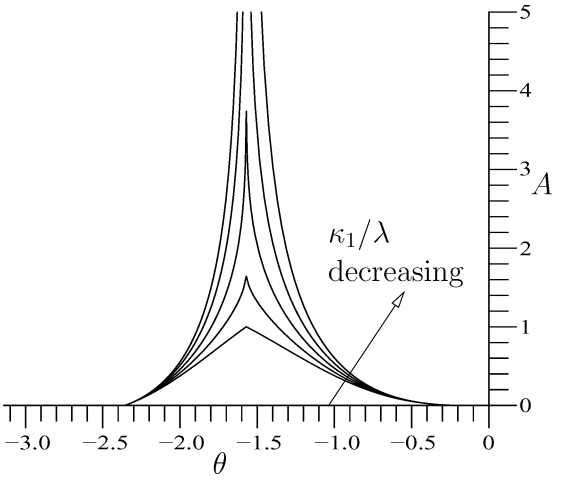

FIGURE 4. The amplitude A of the leading-order solution $c_0^{(I)}$ in region I for $\gamma^+ = \pi/16,\ \gamma^- = \pi/4,\ \hat{\Omega} = 1,\ \alpha = 0$ and for $\kappa_1/\lambda = 0.4,\ 0.8,\ 1.2,\ 1.6,\ 2.0$.

$\epsilon \ll \kappa \ll 1$, so that we can write $\kappa = \epsilon^\mu \kappa_\mu$ with $0 < \mu < 1$, the concentration in region I satisfies

$$c^{(I)} \sim \frac{\hat{A}(\theta - \hat{\alpha}(z), z)}{\epsilon^\mu} \exp(-\hat{\Omega}(z) \sin(\hat{\alpha}(z) - \theta) R),$$

where

$$\hat{A}(\psi, z) = \begin{cases} 0 & \text{for} \quad 0 > \psi > -\gamma^+, \\ \lambda \hat{\Omega}(z) \sin(-\psi)/\kappa_\mu & \text{for} \quad -\pi + \gamma^- < \psi < -\gamma^+, \\ 0 & \text{for} \quad -\pi < \psi < -\pi + \gamma^-. \end{cases}$$

This corresponds to a solution in which the azimuthal flux around the edge of the tube is negligible, with most material being absorbed, from the boundary layer, directly onto the adjacent section of vessel wall before it can be advected a significant distance azimuthally. This result may be obtained directly from (3.16) by substituting $\kappa_1 = \epsilon^{\mu-1}\kappa_\mu$, taking the leading term in ϵ and substituting the result back into (3.10).

3.2.2 *Region II: the inner layer about the curve C*

In the case $\kappa_1/\lambda < 1$, in which the solution for $c^{(I)}$ becomes infinite along $\theta = -\pi/2 + \hat{\alpha}(z)$ (see (3.16) and (3.10)) we consider a further layer about $\theta = -\pi/2 + \hat{\alpha}(z)$ by introducing the rescaled variable η defined by

$$\theta = -\frac{\pi}{2} + \hat{\alpha}(z) + \epsilon^{1/2}\eta. \tag{3.18}$$

In this region a balance exists between advection and diffusion in the θ direction (note that in region I diffusion is negligible). In terms of η and the long-time variable $\tau = \epsilon t$,

https://doi.org/10.1017/S0956792509990155 Published online by Cambridge University Press

(2.7) can be rewritten as

$$\epsilon^2(1-\epsilon R)\frac{\partial c^{(II)}}{\partial \tau}-\frac{\partial}{\partial R}\left((1-\epsilon R)J_r^{(II)}\right)$$
$$+\epsilon^{1/2}\frac{\partial J_\theta^{(II)}}{\partial \eta}-\epsilon^{1/2}\frac{d\hat{\alpha}}{dz}(1-\epsilon R)\frac{\partial J_z^{(II)}}{\partial \eta}+\epsilon(1-\epsilon R)\frac{\partial J_z^{(II)}}{\partial z}=0, \tag{3.19}$$

$$\frac{J_r^{(II)}}{\lambda} = (1-\epsilon R)\frac{\partial c^{(II)}}{\partial R}+\hat{\Omega}(z)\left(1-\frac{1}{2}\epsilon\eta^2\right)c^{(II)}+O(\epsilon^{3/2}c^{(II)}), \tag{3.20}$$

$$\frac{J_\theta^{(II)}}{\lambda} = -\epsilon^{1/2}\left(\frac{\partial c^{(II)}}{\partial \eta}+\hat{\Omega}(z)\eta c^{(II)}\right)+\epsilon^{3/2}\hat{\Omega}(z)\left(\frac{\eta^3}{6}+\Delta a_1(z)\eta\right)c^{(II)}+O(\epsilon^2 c^{(II)}), \tag{3.21}$$

$$J_z^{(II)} = \epsilon c^{(II)}\left(\lambda\Delta(\hat{W}(z)+O(\epsilon^{3/2}))+(2R-\epsilon R^2)\right), \tag{3.22}$$

where we recall that $\delta=\Delta\epsilon$, $r=1-\epsilon R$ and $\kappa=\epsilon\kappa_1$. In (3.19)–(3.22) we have used (2.14) to expand $\alpha(\boldsymbol{x})$, $W(\boldsymbol{x})$ and $\Omega(\boldsymbol{x})$. The system is closed by imposing the following boundary and matching conditions:

$$J_r^{(II)}|_{R=0}=\kappa_1\epsilon c^{(II)}, \tag{3.23}$$

$$\left.\begin{aligned} J_r^{(II)} &\to -\lambda\hat{\Omega}(z)c_0^{(o)}(1,\theta,z,t)\sin(-\pi/2+\epsilon^{1/2}\eta)\\ c^{(II)} &\to c_0^{(o)}(1,-\pi/2+\hat{\alpha}(z)+\epsilon^{1/2}\eta,z,t)\end{aligned}\right\} \quad \text{as} \quad R\to+\infty, \tag{3.24}$$

$$c^{(II)}\sim\epsilon^{-1-(1-\kappa_1/\lambda)/2}\frac{\hat{\Omega}(z)}{1-\kappa_1/\lambda}\left(\frac{\cos\gamma^{\pm}}{|\eta|}\right)^{1-\kappa_1/\lambda}\exp(-\hat{\Omega}(z)R) \quad \text{as} \quad \eta\to\pm\infty. \tag{3.25}$$

Conditions (3.24) are derived by matching to the outer region (o) and conditions (3.25) by matching to the inner region (I).

Boundary conditions (3.25) give rise to a term in the expansion of $c^{(II)}$ of $O(\epsilon^{-1-(1-\kappa_1/\lambda)/2})$ (the leading term in the expansion) while the conditions (3.24) give a term of $O(1)$ in $c^{(II)}$ (the fourth-order term in the expansion) and the penultimate term in (3.19) leads to an $O(\epsilon^{1-(1-\kappa_1/\lambda)/2})$ term in $J_r^{(II)}$ (the fifth-order term in the expansion). Motivated by these facts and the expectation that the solution in this region is driven by the behaviour in region I, we seek an asymptotic solution of the form

$$\begin{aligned}
c^{(II)} &= \epsilon^{-(1+(1-\kappa_1/\lambda)/2)}\left(c_0^{(II)}+\epsilon^{(1-\kappa_1/\lambda)/2}c_1^{(II)}+\epsilon^{1/2}c_2^{(II)}\right.\\
&\quad\left.+\epsilon c_3^{(II)}+\epsilon^{1+(1-\kappa_1/\lambda)/2}c_4^{(II)}+\epsilon^{3/2}c_5^{(II)}+\cdots\right),\\
J_r^{(II)} &= \epsilon^{-(1+(1-\kappa_1/\lambda)/2)}\left(J_{r,0}^{(II)}+\epsilon^{(1-\kappa_1/\lambda)/2}J_{r,1}^{(II)}+\epsilon^{1/2}J_{r,2}^{(II)}+\epsilon J_{r,3}^{(II)}\right.\\
&\quad\left.+\epsilon^{1+(1-\kappa_1/\lambda)/2}J_{r,4}^{(II)}+\epsilon^{3/2}J_{r,5}^{(II)}+\cdots\right),\\
J_\theta^{(II)} &= \epsilon^{-(1+(1-\kappa_1/\lambda)/2)}\left(\epsilon^{1/2}J_{\theta,0}^{(II)}+\epsilon^{1/2+(1-\kappa_1/\lambda)/2}J_{\theta,1}^{(II)}+\epsilon J_{\theta,2}^{(II)}+\cdots\right),\\
J_z^{(II)} &= \epsilon^{-(1+(1-\kappa_1/\lambda)/2)}\left(\epsilon J_{z,0}^{(II)}+\cdots\right),
\end{aligned}$$

In (3.26) terms denoted by the subscripts 1 and 2 are linked to those denoted by 4 and 5 (discussed above) which excite eigenmodes at higher order. Since we are primarily concerned with the leading-order term we can ignore those denoted by subscripts 1,2,4 and 5. However, since $c_0^{(II)}$ satisfies an eigenvalue problem we need to proceed to the third

https://doi.org/10.1017/S0956792509990155 Published online by Cambridge University Press

order (denoted by subscript 3) in order to obtain a solvability condition which will allow us to specify $c_0^{(II)}$ fully.

Substituting from (3.26) into (3.19) and (3.23)–(3.24a) leads, at leading order, to the result $J_{r,0}^{(II)} = 0$ while (3.20) and (3.24b) once again supply a balance between advective and diffusive flux in the radial direction (at leading order)

$$\frac{\partial c_0^{(II)}}{\partial R} + \hat{\Omega}(z) c_0^{(II)} = 0, \qquad \text{with} \qquad c_0^{(II)} \to 0 \quad \text{as} \quad R \to \infty,$$

with eigensolution

$$c_0^{(II)} = B(\eta, z, \tau) \exp(-\hat{\Omega}(z) R), \tag{3.26}$$

where the amplitude function $B(\eta, z, \tau)$ remains to be found. It turns out, as we shall see, that B is determined by the azimuthal flux of material and the rate of its absorbtion at the vessel wall. Proceeding with the expansions of (3.19) and (3.23)–(3.24a) to third order gives the following problem for $J_{r,3}^{(II)}$

$$\frac{\partial J_{r,3}^{(II)}}{\partial R} = \frac{\partial J_{\theta,0}^{(II)}}{\partial \eta}, \qquad J_{r,3}^{(II)}|_{R=0} = \kappa_1 c_0^{(II)}|_{R=0}, \qquad J_{r,3}^{(II)} \to 0 \quad \text{as} \quad R \to \infty. \tag{3.27}$$

Here $J_{\theta,0}^{(II)}$ is obtained by substituting for $c_0^{(II)}$ in the leading term of (3.21) and is

$$J_{\theta,0}^{(II)} = -\lambda (B_\eta + \hat{\Omega}(z) \eta B) \exp(-\hat{\Omega}(z) R).$$

We obtain a solvability condition on B by integrating (3.27a) between $R = 0$ and $R = \infty$ and applying the boundary conditions (3.27b)–(3.27c); this yields the following second-order DE for B:

$$\frac{1}{\hat{\Omega}(z)} B_{\eta\eta} + \eta B_\eta + B(1 - \kappa_1/\lambda) = 0,$$

with solution

$$B = \exp(-\hat{\Omega}(z)\eta^2/2) \left(\alpha(z,\tau) H_{-\kappa_1/\lambda} \left(\left(\hat{\Omega}(z)/2 \right)^{1/2} \eta \right) + \beta(z,\tau) K_M \left(\frac{\kappa_1}{2\lambda}, \frac{1}{2}, \frac{\hat{\Omega}(z)}{2} \eta^2 \right) \right), \tag{3.28}$$

where $H_\nu(\cdot)$ is the Hermite function of degree ν and $K_M(\cdot,\cdot,\cdot)$ is the hypergeometric Kummer function of the first kind. The functions α and β can be determined from the matching conditions (3.24)–(3.25) which give the following far-field conditions on B:

$$B \sim \frac{\hat{\Omega}(\cos\gamma^-)^{1-\kappa_1/\lambda}}{(1-\kappa_1/\lambda)(-\eta)^{1-\kappa_1/\lambda}} \quad \text{as} \quad \eta \to -\infty, \qquad B \sim \frac{\hat{\Omega}(\cos\gamma^+)^{1-\kappa_1/\lambda}}{(1-\kappa_1/\lambda)\eta^{1-\kappa_1/\lambda}} \quad \text{as} \quad \eta \to \infty. \tag{3.29}$$

The asymptotic behaviours of the Hermite function (of degree $-\kappa_1$) and the Kummer

https://doi.org/10.1017/S0956792509990155 Published online by Cambridge University Press

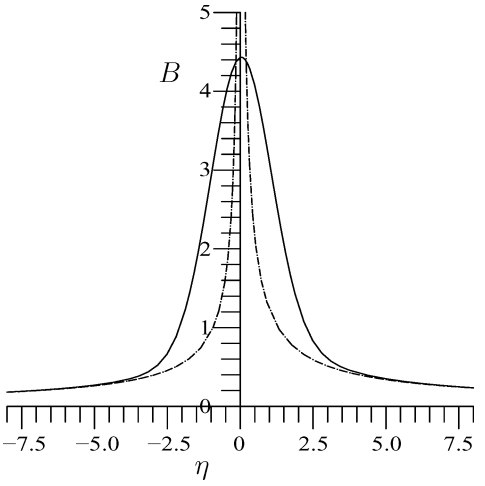

FIGURE 5. Sketch of the amplitude function B inside region II for fixed values of z and τ. Key: $B(\eta)$ for $\Omega = 1$, $\gamma^+ = \Pi/16$, $\gamma^- = \pi/4$ and $\kappa_1/\lambda = 0.2$ (solid line); the asymptotic behaviour as $\eta \to \pm\infty$ (dashed line).

function [30] at infinity are

$$H_{-\kappa_1/\lambda}\left(\left(\hat{\Omega}/2\right)^{1/2}\eta\right) \sim \Gamma(1-\kappa_1/\lambda)\frac{(-\eta)^{\kappa_1/\lambda-1}}{\sqrt{\pi}} \times \sin(\kappa_1\pi/\lambda)\exp\left(\frac{\hat{\Omega}}{2}\eta^2\right)\left(\frac{\hat{\Omega}}{2}\right)^{(\kappa_1/\lambda-1)/2} \quad \text{as} \quad \eta \to -\infty,$$

$$H_{-\kappa_1/\lambda}\left(\left(\hat{\Omega}/2\right)^{1/2}\eta\right) \sim 2^{-\kappa_1/\lambda}\left(\frac{\hat{\Omega}}{2}\right)^{-\kappa_1/\lambda}\eta^{-\kappa_1/\lambda} \quad \text{as} \quad \eta \to \infty,$$

$$K_M\left(\frac{\kappa_1}{2\lambda}, \frac{1}{2}, \frac{\hat{\Omega}}{2}\eta^2\right) \sim \frac{\sqrt{\pi}}{\Gamma(\kappa_1/(2\lambda))}\left(\frac{2}{\hat{\Omega}}\right)^{(1-\kappa_1/\lambda)/2}\exp\left(\frac{\hat{\Omega}}{2}\eta^2\right)|\eta|^{\kappa_1/\lambda-1} \quad \text{as} \quad \eta \to \pm\infty.$$

It follows that, in order to satisfy the far-field conditions (3.29), $\alpha(z,\tau)$ and $\beta(z,\tau)$ in (3.28) must be chosen as follows:

$$\alpha(z,\tau) = \frac{\sqrt{\pi}\hat{\Omega}(z)}{(1-\kappa_1/\lambda)\Gamma(1-\kappa_1/\lambda)\sin(\kappa_1\pi/\lambda)}\left(\frac{\hat{\Omega}(z)}{2}\right)^{(1-\kappa_1/\lambda)/2} \times \left((\cos\gamma^-(z,\tau))^{1-\kappa_1/\lambda} - (\cos\gamma^+(z,\tau))^{1-\kappa_1/\lambda}\right), \tag{3.30}$$

$$\beta(z,\tau) = \frac{\Gamma(\kappa_1/(2\lambda))\hat{\Omega}(z)}{(1-\kappa_1/\lambda)\sqrt{\pi}}\left(\frac{\hat{\Omega}(z)}{2}\right)^{(1-\kappa_1/\lambda)/2}(\cos\gamma^+(z,\tau))^{1-\kappa_1/\lambda}. \tag{3.31}$$

In summary the leading-order concentration $c_0^{(II)}$ is given by (3.26) in which the amplitude $B(\eta,z,\tau)$ is defined by (3.28) and (3.30)–(3.31). A plot of B (solid line) is presented in Figure 5, together with its asymptotic behaviours as $\eta \to \pm\infty$ (dotted lines), these being derived from the amplitude function A in region I.

https://doi.org/10.1017/S0956792509990155 Published online by Cambridge University Press

3.2.3 *Summary and physical interpretation of results in §3.2*

We have considered the distinguished limit in which the vessel aspect ratio and the dimensionless permeability of the vessel wall are both small and of similar magnitude to the inverse Peclet numberϵ ($\delta = O(\epsilon)$, $\kappa = O(\epsilon)$). We find that there is a boundary layer (region I) of dimensionless width $O(\epsilon)$ around the edge of the vessel in which the concentration is $O(1/\epsilon)$ greater than that in the bulk of the vessel (region o). In this boundary layer there is a balance between diffusion which acts to return particles to the centre of the vessel (where concentrations are lower) and advection which pulls particles to the wall. The relatively high concentrations in the boundary layer lead, in this case, to a significant $O(1)$ flux of particles through the vessel wall. Additionally there is an axial flux of particles along the boundary layer, around the edge of the vessel, towards $\theta = -\pi/2 + \hat{\alpha}(z)$ and this results in a further region (region II) of width ϵ in the radial direction and of width $\epsilon^{1/2}$ in the azimuthal direction. Here the particle concentration is of $O(\epsilon^{-(1+(1-\kappa_1/\lambda)/2)})$ and the resulting flux through the vessel wall of $O(\epsilon^{-(1-\kappa_1/\lambda)/2})$. The integrated flux of particles leaving through the vessel wall, per unit length in the z direction, in region II, which we denote by $J_w^{(II)}$, is thus of $O(\epsilon^{\kappa_1/(2\lambda)})$ which is negligible in comparison to the integrated flux of particles through the vessel wall, per unit length in the z direction, occurring in region I, which we denote by $J_w^{(I)}$, and which is $O(1)$. Indeed an expression for the latter is given by

$$J_w^{(I)} = \kappa_1 \int_{-\pi+\hat{\alpha}}^{\hat{\alpha}} J_r^{(I)}|_{R=0} \mathrm{d}\psi \sim \int_{-\pi+\hat{\alpha}}^{\hat{\alpha}} c_0^{(I)}|_{R=0} \mathrm{d}\psi = \kappa_1 \int_{-\pi+\hat{\alpha}}^{\hat{\alpha}} A(\psi, z) \mathrm{d}\psi.$$

After performing the integration this expression may be rewritten in the form

$$J_w^{(I)} \sim \lambda \hat{\Omega}(z)(\cos\gamma^-(z) + \cos\gamma^+(z)).$$

We can interpret this as a statement that the flux of particles leaving through the wall (per unit length in the z direction) is asymptotic to the flux entering the boundary layers from the outer region. It can thus be seen that the processes occurring in region I are of much greater practical interest than those occurring in region II. It is notable that, in this regime, no significant flux of particles occurs down the vessel, in the z direction, in either boundary layer region I or II. Given that the problem is quasi-steady in the outer region and in region I over the $O(1/\epsilon)$ timescale being investigated, it is thus not surprising that the flux out of the outer is equal to that being absorbed on the wall.

Breakdown of the expansion as $\kappa_1/\lambda \to 0$.

The solution in region II breaks down in the limit $\kappa_1/\lambda \to 0$, because the coefficients α and β defined in (3.30)–(3.31) blow up, giving the small κ_1/λ behaviour

$$B \sim \exp(-\hat{\Omega}\eta^2/2)\frac{\lambda\hat{\Omega}^{3/2}}{(2\pi)^{1/2}\kappa_1}(\cos\gamma^- + \cos\gamma^+),$$

https://doi.org/10.1017/S0956792509990155 Published online by Cambridge University Press

corresponding to

$$c^{(II)} \sim \epsilon^{-3/2} \exp(-\hat{\Omega}(R + \eta^2/2)) \frac{\lambda \hat{\Omega}^{3/2}}{(2\pi)^{1/2}\kappa_1} (\cos\gamma^- + \cos\gamma^+), \tag{3.32}$$

where we used the facts that $K_M(0, 1/2, x) = H_0(x) = 1$. This motivates us to consider a second distinguished limit for which $\kappa = O(\epsilon^2)$ in Section 3.3.

3.3 The distinguished limit $\delta = O(\epsilon)$, $\kappa = O(\epsilon^2)$ and $\lambda = O(1)$

Here we proceed as before but write $\kappa = \epsilon^2\kappa_2$. Once again the solution in the outer region (o) is unaffected by the boundary condition (2.7e) and may be described by the analysis in Section 3.1.

3.3.1 *Region I: the diffusive boundary layer on the outflow boundary* $-\pi + \hat{\alpha} < \theta < \hat{\alpha}$

The analysis in region I is identical to that in Section 3.2 except with $\kappa_1 = 0$. The concentration thus has the asymptotic expansion $c^{(I)} = c_0^{(I)}/\epsilon + \cdots$. Where the outer solution has the form described in (3.15) the steady solution for $c_0^{(I)}$ takes the form $c_0^{(I)} = A(\theta, z) \exp(-\hat{\Omega}(z) \sin(\hat{\alpha}(z) - \theta)R)$ and $A(\theta, z)$ is given by (3.16) with $\kappa_1 = 0$.

3.3.2 *Region II: the inner boundary layer about the curve C on* $\theta = -\pi/2 + \hat{\alpha}(z)$

We use the stretched variables R and η defined in (3.2) and (3.18) in terms of which the governing equations (2.7) take the form (3.19)–(3.21). However the system is now closed by the boundary conditions

$$J_r^{(II)}|_{R=0} = \kappa_2 \epsilon^2 c^{(II)}, \tag{3.33}$$

$$\left.\begin{aligned} J_r^{(II)} &\to -\lambda \hat{\Omega}(z) c_0^{(o)}(1, \theta, z, t) \sin(-\pi/2 + \epsilon^{1/2}\eta) \\ c^{(II)} &\to c_0^{(o)}(1, -\pi/2 + \hat{\alpha}(z) + \epsilon^{1/2}\eta, z, t) \end{aligned}\right\} \quad \text{as} \quad R \to +\infty, \tag{3.34}$$

$$c^{(II)} \sim \epsilon^{-3/2} \hat{\Omega}(z) \left(\frac{\cos\gamma^-}{-\eta}\right) \exp(-\hat{\Omega}(z)R) \quad \text{as} \quad \eta \to -\infty, \tag{3.35}$$

$$c^{(II)} \sim \epsilon^{-3/2} \hat{\Omega}(z) \left(\frac{\cos\gamma^+}{\eta}\right) \exp(-\hat{\Omega}(z)R) \quad \text{as} \quad \eta \to \infty. \tag{3.36}$$

These are identical to (3.23)–(3.25) with κ_1 replaced by $\epsilon\kappa_2$.

In light of the matching conditions (3.35)–(3.36) we might naively expect that the leading term in $c^{(II)}$ is of $O(\epsilon^{-3/2})$. However, as we have seen in §3.2.2, this scaling breaks down for $\kappa = o(\epsilon)$ and the appropriate scaling in the distinguished limit $\kappa = O(\epsilon^2)$ is $c^{(II)} = O(\epsilon^{-5/2})$. The calculation initially proceeds along similar lines to that in Section 3.2.2 with the dependence of $c_0^{(II)}$ (the leading term in $c^{(II)}$) on R obtained at leading order (i.e. at $O(\epsilon^{-5/2})$) giving $c_0^{(II)} = F(\eta, z, \tau) \exp(-\hat{\Omega}(z)R)$. The η-dependence of the amplitude $F(\eta, z, \tau)$ is derived from a solvability condition at $O(\epsilon^{-3/2})$ while, in contrast to Section 3.2.2, the dependence of F on z and τ is found by proceeding to $O(\epsilon^{-1/2})$ and obtaining a further solvability condition. However since, in general, the direction of the force on

https://doi.org/10.1017/S0956792509990155 Published online by Cambridge University Press

the particles changes with z (corresponding to a non-zero derivative of $\hat{\alpha}(z)$) we must also consider terms in $c^{(II)}$ at orders ϵ^{-2}, ϵ^{-1}, etc. Furthermore these terms appear in the equations used to derive the second solvability condition on $F(\eta, z, \tau)$, although they do not affect the final result for $F(\eta, z, \tau)$. The essence of this calculation can therefore be best obtained by ignoring the terms in $c^{(II)}$ at integer powers of ϵ (corresponding to the assumption that $\hat{\alpha}'(z) = 0$) and concentrating solely on those terms at half-integer powers of ϵ.

Motivated by the above discussion we look for an expansion of the form

$$\begin{aligned}
c^{(II)} &= \epsilon^{-5/2}c_0^{(II)} + \epsilon^{-2}c_1^{(II)} + \epsilon^{-3/2}c_2^{(II)} + \epsilon^{-1}c_3^{(II)} + \epsilon^{-1/2}c_4^{(II)} + \cdots,\\
J_r^{(II)} &= \epsilon^{-5/2}J_{r,0}^{(II)} + \epsilon^{-2}J_{r,1}^{(II)} + \epsilon^{-3/2}J_{r,2}^{(II)} + \epsilon^{-1}J_{r,3}^{(II)} + \epsilon^{-1/2}J_{r,4}^{(II)} + \cdots,\\
J_\theta^{(II)} &= \epsilon^{-2}J_{\theta,0}^{(II)} + \epsilon^{-3/2}J_{\theta,1}^{(II)} + \epsilon^{-1}J_{\theta,2}^{(II)} + \cdots,\\
J_z^{(II)} &= \epsilon^{-3/2}J_{z,0}^{(II)} + \epsilon^{-1}J_{z,1}^{(II)} + \epsilon^{-1/2}J_{z,2}^{(II)} + \cdots.
\end{aligned} \tag{3.37}$$

At the two leading orders the governing equations (3.19)–(3.20) and boundary conditions (3.33)–(3.34) are identical to those in Section 3.2.2. In particular,

$$J_{r,0}^{(II)} = J_{r,1}^{(II)} = 0, \quad c_0^{(II)} = F(\eta, z, \tau)\exp(-\hat{\Omega}(z)R), \quad c_1^{(II)} = G(\eta, z, \tau)\exp(-\hat{\Omega}(z)R), \tag{3.38}$$

where the amplitude functions F and G remain to be determined. At $O(\epsilon^{-3/2})$ and $O(\epsilon^{-1})$ in (3.19) we obtain

$$\frac{\partial J_{r,2}^{(II)}}{\partial R} = \frac{\partial J_{\theta,0}^{(II)}}{\partial \eta}, \qquad \frac{\partial J_{r,3}^{(II)}}{\partial R} = \frac{\partial J_{\theta,1}^{(II)}}{\partial \eta} - \frac{\mathrm{d}\hat{\alpha}}{dz}\frac{\partial J_{z,0}^{(II)}}{\partial \eta}, \tag{3.39}$$

where $(J_{\theta,0}^{(II)}, J_{\theta,1}^{(II)}, J_{z,0}^{(II)})$ are determined from the solutions for $c_0^{(II)}$ and $c_1^{(II)}$ by expanding (3.21) and (3.22) to the appropriate order

$$J_{\theta,0}^{(II)} = -\lambda\left(\hat{\Omega}(z)c_0^{(II)}\eta + \frac{\partial c_0^{(II)}}{\partial \eta}\right), \qquad J_{z,0}^{(II)} = c_0^{(II)}(\lambda\Delta\hat{W}(z) + 2R), \tag{3.40}$$

$$J_{\theta,1}^{(II)} = -\lambda\left(\hat{\Omega}(z)c_1^{(II)}\eta + \frac{\partial c_1^{(II)}}{\partial \eta}\right), \qquad J_{z,1}^{(II)} = c_1^{(II)}(\lambda\Delta\hat{W}(z) + 2R). \tag{3.41}$$

Boundary conditions on $J_{r,2}^{(II)}$ and $J_{r,3}^{(II)}$ are derived from the $O(\epsilon^{-5/2})$ and $O(\epsilon^{-3/2})$ terms that appear in (3.33)–(3.34)

$$\left.\begin{aligned} J_{r,2}^{(II)}|_{R=0} &= 0\\ J_{r,2}^{(II)} &\to 0 \quad \text{as} \quad R \to \infty \end{aligned}\right\}, \qquad \left.\begin{aligned} J_{r,3}^{(II)}|_{R=0} &= 0\\ J_{r,3}^{(II)} &\to 0 \quad \text{as} \quad R \to \infty \end{aligned}\right\}. \tag{3.42}$$

Substituting from (3.40)–(3.41) for $(J_{\theta,0}^{(II)}, J_{\theta,1}^{(II)}, J_{z,0}^{(II)})$ in (3.39), integrating with respect to R, and applying boundary conditions (3.42) gives the following solvability conditions for F and G:

$$\frac{\partial}{\partial \eta}\left(F_\eta + \hat{\Omega}(z)\eta F\right) = 0, \qquad \frac{\partial}{\partial \eta}\left(G_\eta + \hat{\Omega}(z)\eta G\right) = -\frac{\mathrm{d}\hat{\alpha}}{\mathrm{d}z}\left(\Delta W + \frac{2}{\lambda\Omega}\right)F_\eta. \tag{3.43}$$

https://doi.org/10.1017/S0956792509990155 Published online by Cambridge University Press

Boundary conditions on (3.43) can be obtained from the matching conditions (3.35)–(3.36) and are

$$F \to 0 \quad \text{and} \quad G \to 0 \qquad \text{as} \quad \eta \to \pm\infty.$$

Integrating (3.43a) subject to the above boundary conditions yields

$$F(\eta, z, \tau) = f(z, \tau)\exp(-\hat{\Omega}(z)\eta^2/2) \Longrightarrow c_0^{(II)} = f(z, \tau)\exp(-\hat{\Omega}(z)(R + \eta^2/2)), \tag{3.44}$$

where the amplitude function $f(z, \tau)$ is determined below. Similarly integration of (3.43b) subject to the above boundary conditions on G gives (on substituting for F using (3.44))

$$G = -\frac{\mathrm{d}\hat{\alpha}}{\mathrm{d}z}\left(\Delta\hat{W}(z) + \frac{2}{\lambda\hat{\Omega}(z)}\right) f(z, \tau)\eta\exp(-\hat{\Omega}(z)\eta^2/2).$$

These results lead to the following expressions for the fluxes in the azimuthal and axial directions:

$$\begin{aligned}
&J_{\theta,0}^{(II)} = 0 \qquad J_{z,0}^{(II)} = f(z, \tau)(\lambda\Delta\hat{W}(z) + 2R)\exp(-\hat{\Omega}(z)(R + \eta^2/2)),\\
&J_{\theta,1}^{(II)} = \lambda\frac{\mathrm{d}\hat{\alpha}}{\mathrm{d}z}\left(\Delta\hat{W} + \frac{2}{\lambda\hat{\Omega}}\right) f(z, \tau)\exp(-\hat{\Omega}(z)(R + \eta^2/2)),\\
&J_{z,1}^{(I)} = -\frac{\mathrm{d}\hat{\alpha}}{\mathrm{d}z}(\lambda\Delta\hat{W}(z) + 2R)(\lambda\Delta\hat{W}(z) + 2/\hat{\Omega})\eta f(z, \tau)\exp(-\hat{\Omega}(z)(R + \eta^2/2))
\end{aligned} \tag{3.45}$$

and furthermore that the solution to (3.39a) with (3.42a) is $J_{r,2}^{(II)} = 0$.

In order to determine f we must first calculate $J_{\theta,2}^{(II)}$ by proceeding to $O(\epsilon^{-1})$ in (3.21), where we find

$$J_{\theta,2}^{(II)} = -\lambda\left(\left(\frac{\partial}{\partial\eta} + \hat{\Omega}(z)\eta\right) c_2^{(II)} - \hat{\Omega}(z)\left(\frac{\eta^3}{6} + \Delta a_1(z)\eta\right) c_0^{(II)}\right). \tag{3.46}$$

By proceeding to $O(\epsilon^{-3/2})$ in (3.20) and recalling that $J_{r,2}^{(II)} = 0$ we obtain the following equation for $c_2^{(II)}$:

$$\frac{\partial c_2^{(II)}}{\partial R} + \hat{\Omega}(z)c_2^{(II)} = R\frac{\partial c_0^{(II)}}{\partial R} + \frac{\hat{\Omega}(z)\eta^2}{2}c_0^{(II)} = f(z, \tau)\hat{\Omega}(z)\left(\frac{\eta^2}{2} - R\right)\exp(-\hat{\Omega}(z)(R + \hat{\Omega}(z)\eta^2/2))$$

with solution

$$c_2^{(II)} = \frac{\hat{\Omega}(z)f(z, \tau)}{2}(\eta^2 R - R^2)\exp(-\hat{\Omega}(z)(R + \eta^2/2)) + g(\eta, z, \tau)\exp(-\hat{\Omega}(z)R), \tag{3.47}$$

where g is an, as yet undetermined, function of integration. Substitution from (3.47) into (3.46), gives the desired expression for $J_{\theta,2}^{(II)}$

$$\begin{aligned}
J_{\theta,2}^{(II)} \;=\; &-\lambda\hat{\Omega}(z)f(z, \tau)\exp\left(-\hat{\Omega}(z)\left(R + \frac{\eta^2}{2}\right)\right)\left(R\eta - \frac{\eta^3}{6} - \Delta a_1(z)\eta\right)\\
&-\lambda(g_\eta + \hat{\Omega}(z)\eta g)\exp(-\hat{\Omega}(z)R).
\end{aligned} \tag{3.48}$$

https://doi.org/10.1017/S0956792509990155 Published online by Cambridge University Press

We derive a solvability condition on $f(z,\tau)$ by proceeding to $O(\epsilon^{-1/2})$ in (3.19) and (3.33)–(3.34). In this way we recover the following problem for $J^{(II)}_{r,4}$:

$$\frac{\partial c_0^{(II)}}{\partial \tau} - \frac{\partial J^{(II)}_{r,4}}{\partial R} + \frac{\partial J^{(II)}_{\theta,2}}{\partial \eta} - \frac{d\hat{\alpha}}{dz}\frac{\partial J^{(II)}_{z,1}}{\partial \eta} + \frac{\partial J^{(II)}_{z,0}}{\partial z} + \frac{\partial}{\partial R}(RJ^{(II)}_{r,2}) = 0, \tag{3.49}$$

$$J^{(II)}_{r,4}|_{R=0} = \kappa_2 f(z,\tau)\exp(-\hat{\Omega}(z)\eta^2), \qquad J^{(II)}_{r,4} \to 0 \quad \text{as} \quad R \to \infty. \tag{3.50}$$

Integrating (3.49) with respect to R gives

$$\int_0^\infty \frac{\partial c_0^{(II)}}{\partial \tau} + \frac{\partial J^{(II)}_{\theta,2}}{\partial \eta} - \frac{\mathrm{d}\hat{\alpha}}{\mathrm{d}z}\frac{\partial J^{(II)}_{z,1}}{\partial \eta} + \frac{\partial J^{(II)}_{z,0}}{\partial z}\mathrm{d}R = \left[J^{(II)}_{r,4} - RJ^{(II)}_{r,2}\right]_0^\infty,$$

while application of boundary conditions (3.42a) and (3.50) and substitution for $c_0^{(II)}$, $J^{(II)}_{z,1}$, $J^{(II)}_{z,0}$ and $J^{(II)}_{\theta,2}$ from (3.44), (3.45) and (3.48) yields

$$\begin{aligned}
&\exp(-\hat{\Omega}\eta^2/2)f_\tau + \lambda\frac{\partial}{\partial\eta}\left(f\exp(-\hat{\Omega}\eta^2/2)\left\{\left(\hat{\Omega}\frac{\eta^3}{6} + \hat{\Omega}\Delta a_1\eta - \eta\right)\right.\right.\\
&\left.\left. + \left(\frac{\mathrm{d}\hat{\alpha}}{\mathrm{d}z}\right)^2\left(\Delta\hat{W} + \frac{2}{\lambda\hat{\Omega}}\right)^2\eta\right\}\right) + \lambda\hat{\Omega}\frac{\partial}{\partial z}\left(\frac{f\exp(-\hat{\Omega}\eta^2/2)}{\lambda\hat{\Omega}}\left(\Delta\hat{W} + \frac{2}{\lambda\hat{\Omega}}\right)\right)\\
&+ \kappa_2\hat{\Omega}f\exp(-\hat{\Omega}\eta^2/2) = \lambda\frac{\partial}{\partial\eta}(g_\eta + \hat{\Omega}\eta g).
\end{aligned} \tag{3.51}$$

In order to complete the calculation, and derive a PDE for $f(z,\tau)$, we use (3.35)–(3.36) to specify the matching conditions on $c_2^{(II)}$

$$\begin{aligned}
c_2^{(II)} &\sim \frac{\hat{\Omega}(z)\cos(\gamma^+(z))}{\eta}\exp(-\hat{\Omega}(z)R) \quad \text{as} \quad \eta \to \infty,\\
c_2^{(II)} &\sim \frac{\hat{\Omega}(z)\cos(\gamma^+(z))}{(-\eta)}\exp(-\hat{\Omega}(z)R) \quad \text{as} \quad \eta \to -\infty.
\end{aligned}$$

These matching conditions imply that

$$\begin{aligned}
g &\sim \frac{\hat{\Omega}(z)\cos(\gamma^+(z))}{\eta} \quad \text{and} \quad g_\eta + \hat{\Omega}(z)\eta g \sim \hat{\Omega}^2(z)\cos(\gamma^+(z)) \quad \text{as} \quad \eta \to \infty,\\
g &\sim \frac{\hat{\Omega}(z)\cos(\gamma^-(z))}{(-\eta)} \quad \text{and} \quad g_\eta + \hat{\Omega}(z)\eta g \sim -\hat{\Omega}^2(z)\cos(\gamma^-(z)) \quad \text{as} \quad \eta \to -\infty.
\end{aligned}$$

By integrating (3.51) with respect to $\eta \in (-\infty,\infty)$ and applying the above conditions on g we obtain the following PDE for f

$$\frac{\partial f}{\partial \tau} + \hat{\Omega}^{3/2}\frac{\partial}{\partial z}\left(\frac{f}{\hat{\Omega}^{3/2}}\left(\lambda\Delta W + \frac{2}{\hat{\Omega}}\right)\right) = \frac{\lambda\hat{\Omega}^{5/2}}{(2\pi)^{1/2}}(\cos\gamma^+ + \cos\gamma^-) - \kappa_2\hat{\Omega}f, \tag{3.52}$$

where f is related to the concentration in region II by

$$c^{(II)} \sim \epsilon^{-5/2}f(z,\tau)\exp(\hat{\Omega}(z)(R + \eta^2/2)).$$

https://doi.org/10.1017/S0956792509990155 Published online by Cambridge University Press

Remarks The conservation equation for material, with concentration f, that is being transported along a channel of area $\mathscr{A}(z)$ with average velocity $\bar{v}$ is

$$f_\tau + \frac{1}{\mathscr{A}}\frac{\partial}{\partial z}(\bar{v}\mathscr{A}f) = \frac{S}{\mathscr{A}} \tag{3.53}$$

where S is the source of the material per unit length (of channel). Comparing (3.53) to (3.52) we can identify $\mathscr{A}$ with $\hat{\Omega}^{-3/2}$, the average velocity $\bar{v}$ with $\lambda\Delta W + 2/\hat{\Omega}$ and S with $\lambda\hat{\Omega}(2\pi)^{-1/2}(\cos\gamma^+ + \cos\gamma^-) - \kappa_2\hat{\Omega}^{-1/2}$. It is intuitively obvious why $\mathscr{A}$ should scale with $\hat{\Omega}^{-3/2}$ since the leading-order solution $c_0^{(II)}$ decays with length scale $\hat{\Omega}^{-1}$ in the radial direction and with length scale $\hat{\Omega}^{-1/2}$ in the azimuthal direction. The two terms, $\lambda\Delta W$ and $2/\hat{\Omega}$, in the average velocity $\bar{v}$ represent the contributions to the axial particle velocity from the action of the body force and from the fluid flow, respectively. The second of these terms scales with $\hat{\Omega}^{-1}$ because the radial thickness of region II scales with $\hat{\Omega}^{-1}$ while the fluid velocity is proportional to distance from the vessel wall. The first term in S represents the flux of material transported into region II from region I. This scales with $\lambda\hat{\Omega}$ since the advective velocity of material onto the vessel wall also scale s with $\lambda\hat{\Omega}$ while it scales with $(\cos\gamma^+ + \cos\gamma^-)$ since this is the width, measured perpendicular to the body force, of that part of the outer region in which the concentration is non-zero. The final term in S represents the material transported out through the walls of the vessel and this scales with $\hat{\Omega}^{-1/2}$ since the width of region II in the azimuthal direction, and hence the length of boundary on which particle deposition takes place, is proportional to $\hat{\Omega}^{-1/2}$.

In this distinguished limit the flux of particles $J_w^{(I)}$ leaving through the wall in region I (per unit length in the z direction) is of $O(\epsilon\log(1/\epsilon))$ whereas that leaving through the wall in region II, $J_w^{(II)}$, is of $O(1)$. An expression for the latter is given by

$$J_w^{(II)} = \epsilon^{1/2}\int_{-\infty}^{\infty} J_r^{(II)}|_{R=0}\mathrm{d}\eta = \epsilon^{5/2}\int_{-\infty}^{\infty}\kappa_2 c^{(II)}|_{R=0}\mathrm{d}\eta \sim \kappa_2\int_{-\infty}^{\infty} c_0^{(II)}|_{R=0}\mathrm{d}\eta.$$

Substituting for $c_0^{(II)}$ from (3.44) and performing the integration we obtain the result that

$$J_w^{(II)} \sim \kappa_2\frac{(2\pi)^{1/2}}{\hat{\Omega}^{1/2}}f(z,\tau),$$

where $f(z,\tau)$ is the amplitude function for $c_0^{(II)}$. Notably the flux of particles leaving through the walls, per unit length in the z direction, is not the same as that entering the boundary layers from the outer region $\lambda\hat{\Omega}(z)(\cos\gamma^-(z) + \cos\gamma^+(z))$. This is a consequence of a significant flux of particles flowing in the axial direction in region II. Another notable and counterintuitive point is that the particle flux through the walls of the vessel is inversely proportional to the square root of the strength of the particle body force onto the vessel wall $\hat{\Omega}^{1/2}$. As alluded to earlier, this is because the length of wall (per unit length in the z direction) in contact with region II scales like $\hat{\Omega}^{-1/2}$ (strong particle body forces lead to a small contact regions). However it should be emphasised that the flux of particles leaving the outer region is proportional to the strength of the particle body force $\lambda\hat{\Omega}$.

https://doi.org/10.1017/S0956792509990155 Published online by Cambridge University Press

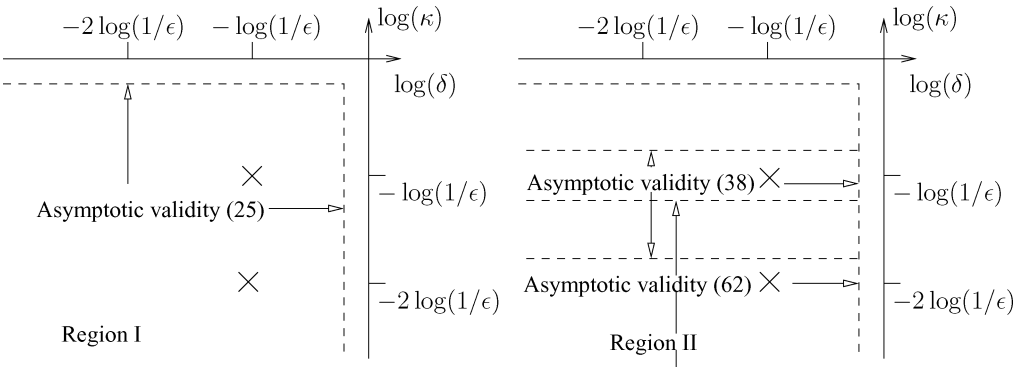

FIGURE 6. Sketches illustrating the asymptotic validity of the asymptotic formulae derived in this paper. The crosses mark the positions of the two distinguished limits considered.

3.3.3 *Limits and validity of (3.52)*

We note first that the large κ_2 limit of (3.52) gives

$$c^{(II)} \sim \frac{\epsilon^{-5/2}}{\kappa_2}\frac{\hat{\Omega}^{3/2}}{(2\pi)^{1/2}}(\cos\gamma^+ + \cos\gamma^-)\exp(-\hat{\Omega}(z)(R+\eta^2/2)),$$

which, giventhat $\kappa_1 = \epsilon\kappa_2$, matches to the small κ_1 limit of the equivalent result in the distinguished limit $\delta = O(\epsilon)$ and $\kappa = O(\epsilon)$ (see (3.32)).

The results obtained in Section 3.3 have considerably wider applicability than the limit $\kappa = O(\epsilon^2)$ and $\delta = O(\epsilon)$. Thus, for example, where $\kappa = \epsilon^{\alpha+1}\kappa_{\alpha+1}$ and $\delta = \Delta_\alpha\epsilon^\alpha$, with $0 < \alpha < 1$, (3.52) is valid in the large Δ limit. That is,

$$c^{(II)} \sim \epsilon^{-3/2-\alpha}\exp(-\hat{\Omega}(z)(R+\eta^2/2))f_\alpha(z,T),$$

where $t = \epsilon^{-\alpha}T$ and

$$\frac{\partial f_\alpha}{\partial T} + \lambda\hat{\Omega}^{3/2}\Delta_\alpha\frac{\partial}{\partial z}\left(\frac{f_\alpha W}{\hat{\Omega}^{3/2}}\right) = \frac{\lambda\hat{\Omega}^{5/2}}{(2\pi)^{1/2}}(\cos\gamma^+ + \cos\gamma^-) - \kappa_{\alpha+1}\hat{\Omega}f_\alpha.$$

This can be seen by substituting

$$f = \epsilon^{1-\alpha}f_\alpha, \quad \kappa_2 = \epsilon^{\alpha-1}\kappa_{\alpha+1}, \quad \Delta = \epsilon^{\alpha-1}\Delta_\alpha \quad \text{and} \quad \tau = \epsilon^{1-\alpha}T$$

(with $0 < \alpha < 1$) and taking the leading terms in ϵ.

We also remark that (3.52) remains valid, if either (or both) of κ_2 or Δ are small or if $\lambda \gg 1$. Thus the analysis in Section 3.3 can also be seen to describe the limits (a) $\kappa = o(\epsilon^2)$, $\delta = O(\epsilon)$, $\lambda = O(1)$, (b) $\kappa = O(\epsilon^2)$, $\delta = o(\epsilon)$, $\lambda = O(1)$ and (c) $\kappa = o(\epsilon^2)$, $\delta = o(\epsilon)$, $\lambda = O(1)$. We will investigate the small λ limit in the following section. The domains of validity are plotted in figure 6.

https://doi.org/10.1017/S0956792509990155 Published online by Cambridge University Press

3.3.4 *Steady solution to (3.52)*

There is an analytic solution to the first-order ODE which results from setting the time-derivative to zero in (3.52). This is

$$f(z) = \frac{\hat{\Omega}^{5/2}(z)}{\hat{\Omega}(z)\lambda\Delta\hat{W}(z)+2}\exp\left(-\int_0^z \frac{\kappa_2(\zeta)\hat{\Omega}^2(\zeta)}{\hat{\Omega}(\zeta)\lambda\Delta\hat{W}(\zeta)+2}\mathrm{d}\zeta\right)$$
$$\times\left(A_0+\int_0^z\left\{\frac{\lambda\hat{\Omega}(\zeta)}{(2\pi)^{1/2}}(\cos\gamma^+(\zeta)+\cos\gamma^-(\zeta))\exp\left(-\int_0^\zeta\frac{\kappa_2(\xi)\hat{\Omega}^2(\xi)}{\hat{\Omega}(\xi)\lambda\Delta\hat{W}(\xi)+2}\mathrm{d}\xi\right)\right\}\mathrm{d}\zeta\right),$$

where A_0 is a constant of integration. We note that this solution exhibits singularities if $(\hat{\Omega}(z)\lambda\Delta\hat{W}(z)+2)$ changes sign.

4 Matched asymptotic solution for small inverse Peclet number ($\epsilon \ll 1$) and small trapping efficiency within the vessel ($\lambda = O(\epsilon)$)

Here we consider distinguished limits in which both the inverse Peclet number and λ are small and of $O(\epsilon)$. The analysis is similar in form to that presented in Section 3. Once again there is an outer region which occupies the bulk of the pipe in which advection dominates. There is also a region an $O(\epsilon)$ distance from the wall of the pipe in which advection and diffusion balance (region I). As in the previous limits, material is transported around the boundary layer towards the curve C (as illustrated in Figure 2) where there is a further layer (region II). However, in the $\lambda = O(\epsilon)$, regime transport takes place in *both* the θ and z directions.

4.1 Solution structure in the outer region

As in Section 3 the outer expansion takes the form $c^{(o)} = c_0^{(o)}+\epsilon c_1^{(o)}+\cdots$, $\quad J_r^{(o)} = \epsilon J_{r,0}^{(o)}+\cdots$. However, since $\lambda \ll 1$, the leading-order governing equations now take the form

$$\frac{\partial c_0^{(o)}}{\partial t}+(1-x^2-y^2)\frac{\partial c_0^{(o)}}{\partial z}=0, \qquad J_{r,0}^{(o)} = -\Lambda\hat{\Omega}(z)\sin(\theta-\hat{\alpha}(z))c_0^{(o)}$$

and in the long-time limit admit solutions of the form $c_0^{(o)} = c_0^{(o)}(x,y)$. Thus, to leading order, the concentration profile that enters the vessel is unchanged throughout the length of the vessel.

4.2 The distinguished limit $\kappa = O(\epsilon)$ and $\delta = O(\epsilon)$

Here we write $\delta = \Delta\epsilon$, $\kappa = \epsilon\kappa_1$ and $\lambda = \epsilon\Lambda$.

Region I.

Here we expect the azimuthal (and radial) fluxes to be of size $O(\epsilon)$ relative to those in the $\lambda = O(1)$ regime; this motivates us to rescale time with ϵ by writing $t = \tau/\epsilon$. The

https://doi.org/10.1017/S0956792509990155 Published online by Cambridge University Press

governing equations and boundary conditions then take the form

$$\epsilon(1-\epsilon R)\frac{\partial c^{(I)}}{\partial \tau} - \frac{1}{\epsilon}\frac{\partial}{\partial R}\left((1-\epsilon R)J_r^{(I)}\right) + \frac{\partial J_\theta^{(I)}}{\partial \theta} + (1-\epsilon R)\frac{\partial J_z^{(I)}}{\partial z} = 0, \qquad \text{where} \tag{4.1}$$

$$J_r^{(I)} = \Lambda\epsilon\left(\frac{\partial c^{(I)}}{\partial R} + \hat{\Omega}(z)\sin(\hat{\alpha}(z)-\theta)c^{(I)}\right) + O(\epsilon^2 c^{(I)}), \tag{4.2}$$

$$J_\theta^{(I)} = -\Lambda\epsilon\hat{\Omega}(z)\cos(\hat{\alpha}(z)-\theta)c^{(I)} + O(\epsilon^2 c^{(I)}), \tag{4.3}$$

$$J_z^{(I)} = 2\epsilon R c^{(I)} + O(\epsilon^2 c^{(I)}), \tag{4.4}$$

$$\text{subject to} \qquad J_r^{(I)}|_{R=0} = \kappa_1 \epsilon c^{(I)}, \tag{4.5}$$

$$\text{and} \qquad c^{(I)} \to c_0^{(o)}(1,\theta,z,t) \quad \text{as} \quad R \to +\infty. \tag{4.6}$$

In the limit $\epsilon \to 0$ the expansion of variables proceeds as follows:

$$c^{(I)} = \frac{c_0^{(I)}}{\epsilon} + c_1^{(I)} + \cdots, \quad J_r^{(I)} = J_{r,0}^{(I)} + \epsilon J_{r,1}^{(I)} + \cdots, \quad J_\theta^{(I)} = J_{\theta,0}^{(I)} + \cdots, \quad J_z^{(I)} = J_{z,0}^{(I)} + \cdots.$$

Here the scaling of $c^{(I)}$ is motivated by the facts that the flux from the outer region is of $O(\epsilon)$, the width of the inner region is of $O(\epsilon)$ and we operate over the $O(1/\epsilon)$ timescale defined by τ. To leading order the calculation proceeds along lines similar to those in Section 3.2.1 with the result that

$$J_{r,0}^{(I)} = 0, \qquad c_0^{(I)} = A(\theta,z,\tau)\exp(-\hat{\Omega}(z)\sin(\hat{\alpha}(z)-\theta)R) \tag{4.7}$$

At next order we recover the following system for $J_{r,1}^{(I)}$:

$$\begin{aligned} &\frac{\partial J_{r,1}^{(I)}}{\partial R} = \frac{\partial c_0^{(I)}}{\partial \tau} + \frac{\partial J_{\theta,0}^{(I)}}{\partial \theta} + \frac{\partial J_{z,0}^{(I)}}{\partial z}, \\ &J_{r,1}^{(I)}|_{R=0} = \kappa_1 c_0^{(I)}|_{R=0}, \\ &J_{r,1}^{(I)} \to -\Lambda\hat{\Omega}(z)\sin(\theta-\hat{\alpha}(z))c_0^{(o)}(1,\theta,z,t) \quad \text{as} \quad R \to +\infty. \end{aligned} \tag{4.8}$$

By noting that the leading-order azimuthal and axial fluxes are given by

$$J_{\theta,0}^{(I)} = -\Lambda\hat{\Omega}(z)\cos(\hat{\alpha}(z)-\theta)c_0^{(I)}, \qquad J_{z,0}^{(I)} = 2Rc_0^{(I)},$$

integrating (4.8a) between $R = 0$ and $+\infty$ and applying the boundary conditions on $J_{r,1}^{(I)}$ we obtain the following equation for the amplitude function $A(\theta,z,\tau)$:

$$\begin{aligned} &\frac{1}{\hat{\Omega}(z)\sin(\hat{\alpha}(z)-\theta)}\frac{\partial A}{\partial \tau} - \Lambda\frac{\partial}{\partial \theta}\left(\frac{\cos(\hat{\alpha}(z)-\theta)}{\sin(\hat{\alpha}(z)-\theta)}A\right) + \frac{\partial}{\partial z}\left(\frac{2A}{\hat{\Omega}^2(z)\sin^2(\hat{\alpha}(z)-\theta)}\right) \\ &\quad = (\Lambda\hat{\Omega}(z)c_0^{(o)}|_{r=1}\sin(\hat{\alpha}(z)-\theta) - \kappa_1(z)A). \end{aligned} \tag{4.9}$$

The time-independent version of (4.9) has characteristic projections of the form

$$z = z_0 + \frac{2}{\Lambda\hat{\Omega}^2(z)}\log|\cot(2\hat{\alpha}(z)-2\theta) - \operatorname{cosec}(2\hat{\alpha}(z)-2\theta)|.$$

https://doi.org/10.1017/S0956792509990155 Published online by Cambridge University Press

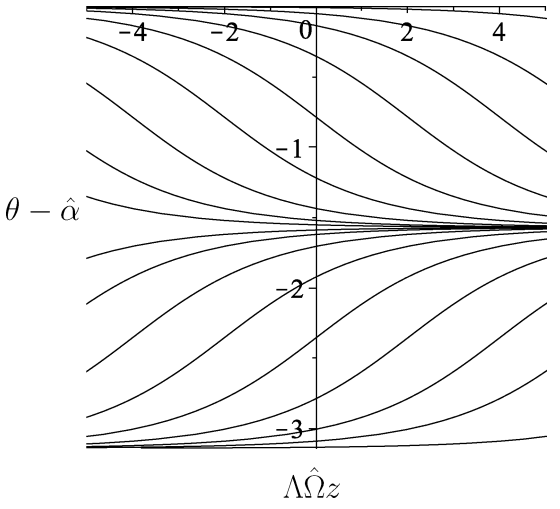

FIGURE 7. The characteristic projections of the steady amplitude equations with $\lambda = O(\epsilon)$ and where both $\hat{\alpha}$ and $\hat{\Omega}$ are independent of z.

where $\hat{\alpha}$ and $\hat{\Omega}$ are independent of z; these are plotted in Figure 7. In this case we note that the amplitude equation in region I is regular. There is therefore no need to introduce a second layer in the neighbourhood of $\theta = \hat{\alpha}(z) - \pi/2$, thus obviating the need for region II.

5 Conclusions

We have developed and analysed a mathematical model describing the transport of a dilute suspension of particles that are subject to a body force and mixed with a second (concentrated) suspension of neutrally buoyant particles that flows through a cylindrical vessel. This problem is relevant to magnetically targeted drug and gene delivery whereby therapeutic drugs and/or genes are attached to biocompatible magnetic nanoparticles, or magnetically loaded macrophages and injected into the blood (a concentrated suspension of red blood cells). A magnetic force is then applied with the aim of guiding the magnetic particles/macrophages to a target site [12, 18, 19, 20, 21]. The body force exerted on the particles leads to them being transported with velocities significantly different to that of the flow and, in particular, to a trans-stream component of velocity that can enhance their deposition on the vessel wall. The presence of the second particulate species (RBCs in our application) introduces a diffusive component to the motion of the first species; such shear induced diffusion is a result of interparticle interactions that occur in sheared flows of concentrated suspensions).

We formulated an advection–diffusion equation to model the transport of the first species. The key dimensionless parameter in the governing transport equations is the inverse Peclet number ϵ which gives the ratio of diffusive effects to advective effects. Guided by dimensional analysis in the case of magnetic targeting we assumed this parameter to be small, which corresponds to a body force that is sufficiently strong to pull the particles into a highly concentrated state in a boundary layer (region I) lying along

https://doi.org/10.1017/S0956792509990155 Published online by Cambridge University Press

the edge of the vessel. Despite the apparent simplicity of the model this regime displays a rich asymptotic structure. In the limit of small particle trapping efficiency $\lambda = O(\epsilon)$ (see Section 4) particles are transported around this boundary layer by the body force, moving in both azimuthal and axial directions, towards the 'bottom' of the vessel (as defined by the particle force). For significant particle trapping efficiency $\lambda = O(1)$ (see Section 3) particle transport within the boundary layer is directed, in a purely azimuthal direction, towards the 'bottom' of the vessel. Here there is a further boundary layer (region II) in which the particle concentration is even greater than in region I. Depending on the relation between ϵ and the permeability $\tilde{\kappa}$ of the vessel wall there may be significant axial transport of particles in this layer along the 'bottom' of the vessel. In the case where this transport is significant (low permeability $\tilde{\kappa}$) we used asymptotic methods to systematically derive an advection equation for the particle concentration within the boundary layer which is represented in dimensionless form in (3.52). This equation can be used to track the flux of particles in the rivulet lying along the 'bottom' of the vessel.

There are several obvious extensions to this work. For example we have only considered a single vessel and, if we are to apply this approach to targeting in the cardiovascular circulation, it would be more realistic to consider a branching network of vessels; this is feasible but the solution to the outer problem is computationally intensive (Grief personal communication [13]). However, once this is accomplished, the numerical solution to the inner problem(s) throughout the network is fairly straightforward. In this context we mention that, except in the limit of weak targeting, particle distributions within networks can be highly heterogeneous [14] *even* within the targeted region. In addition we have not modelled the effects of lift on the red blood cells away from the vessel wall. This creates a RBC-depleted marginal layer lying at the edge of a vessel (typical width 2–4 μm [17]) in which shear-induced diffusion is (presumably) reduced and which will also lead to an additional outwardly directed radial force on the targeted particles in opposition to the lift on RBCs away from the vessel wall (this force is observed on platelets and other small blood borne particles [26]). Furthermore, we have omitted from our discussion the effect of the vessel wall on the particle motion which becomes significant when the particle is a distance of the order of its radius from the vessel wall; these are treated in considerable detail for a spherical particle in [10]. Finally, we have not accounted either for the pulsatile nature of blood flow in arteries [29] or for the orderly single file flow of RBCs which occurs in the smallest capillaries.

We conclude with some observations on magnetic targeting in the cardiovascular circulation. The most important, and perhaps rather obvious comment, concerns the permeability $\tilde{\kappa}$ of the vessel wall to targeted particles. It is apparent from the analysis presented in this paper that this parameter is extremely important for determining where particles are likely to extravasate. If the particles are being targeted at a site of inflammation the vessel permeability there may be considerably elevated above that in the healthy vasculature where it is known to be very low [17]. It is well attested, for example, that the vascular beds in a tumour are leaky and allow particles of diameter 100 nm to permeate from the vasculature into the tissue. Another way to increase the delivery of non-biological particles to the target is to functionalise the carriers by attaching appropriate ligands to them. In this scenario the magnetic force acts to enhance the concentration of particles in the immediate vicinity of the vessel wall, thereby increasing the number which attach,

via a ligand, and ultimately extravasate. Targeting with magnetic macrophages has the advantage that these already have active sites on their surface which can attach to the vessel wall as well as, perhaps more importantly, having the ability to actively extravasate in response to various chemical stimuli.

Acknowledgements

We gratefully acknowledge the financial support from the BBSRC and thank Drs. Munitta Muthana, Neil Farrow and Craig Murdoch, Profs. Jon Dobson and Claire Lewis for many helpful conversations.

References

[1] Ahluwalia, D. S., Keller, J. B. & Knessl, C. (1998) Advection–diffusion around a curved obstacle. *J. Math. Phys.* **39**, 3694–3710.
[2] Alexiou, C. *et al.* (2001) Magnetic mitoxantrone nanoparticle detection by histology, x-ray and MRI after magnetic tumour targeting. *J. Magn. Magn. Mater.* **225**, 187–193.
[3] Alexiou, C., Jurgons, R., Schmid, R., Hilpert, A., Bergmann, C., Parak, F. & Iro, H. (2005) In vitro and in vivo investigations of targeted chemotherapy with magnetic nanoparticles. *J. Magn. Magn. Mater.* **293**, 389–393.
[4] Bishop, J. J., Popel, A. S., Intaglietta, M. & Johnson, P. C. (2002) Effect of aggregation and shear rate on the dispersion of red blood cells flowing in venules. *Am. J. Physiol. Heart Circ. Physiol.* **283**, H1985–H1996.
[5] Davis, R. H. & Acrivos, A. (1985) Sedimentation of noncolloidal particles at low Reynolds numbers . *Annu. Rev. Fluid Mech.* **17**, 91–118.
[6] Dobson, J. (2006) Magnetic nanoparticles for drug delivery. *Drug Dev. Res.* **67**, 55–60.
[7] Eckstein, E. C., Bailey, D. G. & Shapiro, A. (1977) Self-diffusion of particles in shear flow of a suspension. *J. Fluid Mech.* **79**, 191–208.
[8] Forbes, Z. G., Yellen, B. B., Barbee, K. A. & Friedman, G. (2005) An approach to targeted drug delivery based on uniform magnetic fields. *IEEE Trans. Magn.* **10**, 158–166.
[9] Friedman, G. & Yellen, B. (2003) Magnetic separation and assembly of solid phase in fluids. *Curr. Opin. Colloid Interface Sci.* **39**, 3372–3377.
[10] Goldman, A. J., Cox, R. G. & Brenner, H. (1967) Slow viscous motion of a sphere parallel to a plane wall—II Couette flow. *Chem. Eng. Sci.* **22**, 653–660.
[11] Goldsmith, H. L. (1971) Red cell motions and wall interactions in tube flow. *Fed. Proc.* **30**, 1578.
[12] Goodwin, S., Peterson, C., Hoh, C. & Bittner, C. (1999) Targeting and retention of magnetic targeted carriers (MTCs) enhancing intra-arterial chemotherapy. *J. Magn. Magn. Mater.* **194**, 132–139.
[13] Grief, A. D. *Results of unpublished computational code.*
[14] Grief, A. D. & Richardson, G. (2005) Mathematical modelling of magnetically targeted drug delivery . *J. Magn. Magn. Mater.* **293**, 455–463.
[15] Knessl, C. (2001) On two-dimensional convection-diffusion past a circle. *SIAM J. Appl. Math.* **62**, 310–335.
[16] Leighton, D. & Acrivos, A. (1987) The shear-induced migration of particles in concentrated suspensions. *J. Fluid Mech.* **181**, 415–439.
[17] Levick, J. R. (2000) An Introduction to Cardiovascular Physiology, *Arnold*, UK.
[18] Lubbe, A. S. *et al.* (1996) Clinical experiences with magnetic drug targeting: A phase I study with 4'-epidoxorubicin in 14 patients with advanced solid tumours. *Cancer Res.* **56**, 4686–4693.

[19] Mah, C., Fraites, T. J., Zolutukhin, I., Song, S. H., Flotte, T. R., Dobson, J., Batich, C. & Byrne, B. J. (2002) Improved method of recombinant AAV2 delivery for systemic targeted gene therapy. *Mol. Ther.* **6**, 106–112.

[20] Muthana, M., Scott, S. D., Farrow, N., Morrow, F., Murdoch, C., Grubb, S., Brown, N., Dobson, J. & Lewis, C. E. (2008) A novel magnetic approach to enhance the efficacy of cell-based gene therapies. *Gene Therapy* **15**, 902–910. doi:10.1038/gt.2008.57.

[21] Pankurst, Q. A., Connolly, J., Jones, S. K. & Dobson, J. (2003) Applications of magnetic nanoparticles in biomedicine. *J. Phys. D: Appl. Phys.* **36**, R167–R181.

[22] Pich, J. (1972) Theory of gravitational deposition of particles from laminar flows in channels. *Aerosol Sci.* **3**, 351–361.

[23] Reboux, S., Richardson, G. & Jensen, O. E. (2008) Bond tilting and sliding friction in a model of cell adhesion. *Proc. R. Soc.* A **464**, 447–467.

[24] Taylor, G. I. (1953) Dispersion of soluble matter in a solvent flowing slowly through a tube. *Proc. Roy. Soc.* A **219**, 186–203.

[25] Shraiman, B. I. (1987) Diffusive transport in a Rayleigh–Benard convection cell. *Phys Rev.* A **36**, 261–267.

[26] Uijttewaal, W. S. J., Nijhof, E.-J., Bronkhorst, P. J. H., Hartog, E. D. & Heethaar, R. M. (1993) Near-wall excess of platelets induced by lateral migration of erythrocytes in flowing blood. *Am. J. Physiol.* **33**, H1239–H1244.

[27] Voltairas, P. A., Fotiadis, D. I. & Michalis, L. K. (2002) Hydrodynamics of magnetic targeted drug targeting. *J. Biomech.* **35**, 813–821.

[28] Wilson, M. W., Kerlan, R. K., Findleman, N. A., Venook, A. P., LaBerge, J. M., Koda, J. & Gordon, R. L. (2004) Hepatocellular carcinoma: Regional therapy with a magnetic targeted carrier bound to doxorubicin in a dual MR imaging/conventional angiography suite initial experience with four patients. *Radiology* **230**, 287–293.

[29] Womersley, J. R. (1955) Method for the calculation of velocity, rate of flow and viscous drag in arteries when the pressure gradient is known. *J. Physiol.* **127**, 553–563.

[30] Wolfram website http://functions.wolfram.com/HypergeometricFunctions/

[31] Zhang, W., Stone, H. A. & Sherwood, J. D. (1996) Mass transfer at a microelectrode in channel flow. *J. Chem. Phys.* **100**, 9462–9464.

[32] Zydney, A. L. & Colton, C. K. (1988) Augmented solute transport in the shear flow of a concentrated suspension. *Physicochem. Hydrodyn.* **10**, 77–96.